

# The Evolution of Substructure in Galaxy, Group and Cluster Haloes II: Global Properties

James E. Taylor<sup>1,?</sup> and Arif Babul<sup>2</sup>

<sup>1</sup>Denys Wilkinson Building, 1 Keble Road, Oxford OX1 3RH, United Kingdom

<sup>2</sup>Elliott Building, 3800 Finnerty Road, Victoria, BC, V8P 1A1, Canada

20 March 2024

## ABSTRACT

In a previous paper, we described a new method for including detailed information about substructure in semi-analytic models of dark matter halo formation based on merger trees. In this paper, we present the basic predictions of our full model of halo formation. We first describe the overall properties of substructure in galaxy, group or cluster haloes at the present day. We then discuss the evolution of substructure, and the effect of the mass accretion history of an individual halo on the mass function and orbital grouping of its subhalo population. We show, in particular, that the shape of the subhalo mass function is strongly correlated with the formation epoch of the halo. In a third paper in this series we will compare the results of our semi-analytic method with the results of self-consistent numerical simulations of halo formation.

**Key words:** methods: numerical { galaxies: clusters: general { galaxies: formation { galaxies: haloes { dark matter.

## 1 INTRODUCTION

Following the analysis of the first-year data from the Wilkinson Microwave Anisotropy Probe (WMAP), there is now very strong evidence that the matter content of the Universe is in large part non-baryonic (Spergel et al. 2003). Observations of large scale structure (e.g. Percival et al. 2001; Maller et al. 2003; Tegmark et al. 2004), measurements of weak lensing (e.g. Hoekstra et al. 2002; Van Waerbeke et al. 2002; Jarvis et al. 2003; Hamana et al. 2003; Brown et al. 2003; Rhodes et al. 2004), and modelling of the Lyman-forest (e.g. Croft et al. 2002; Demianski & Doroshkevich 2003; Kim et al. 2004) indicate a power spectrum of density fluctuations in this component continuing to subgalactic scales, and consistent with ‘cold’ dark matter (CDM) models. The implications of the CDM power spectrum for structure formation are well established. Dark matter haloes, the dense regions that surround galaxies, groups and clusters, form from the bottom up, through the merging of progressively larger structures. This process of hierarchical merging has been studied extensively for two decades, and the overall properties of galaxy or cluster haloes formed in this way are now fairly well determined.

To learn more about dark matter, and to search for features in the power spectrum that could reveal new phases

in the evolution of the very early universe, we must push the theory of structure formation to smaller scales. Since the present-day evolution of structure is already nonlinear on the scale of galaxy clusters, it is challenging to make even the simplest predictions on subgalactic scales. The usual approach to the problem is to combine the results of simulations on different scales, using numerical simulations of large (100 Mpc<sup>3</sup> or more) volumes to determine the formation rates and properties of the overall population of dark matter haloes at low resolution (e.g. Kauffmann et al. 1999; Bullock et al. 2001; Gottlober, Klypin, & Kravtsov 2001; Yoshida, Sheth, & Diaferio 2001; Evrard et al. 2002; MATHIS et al. 2002; Wambsganss, Bode & Ostriker 2003; Lin, Jing, & Lin 2003; Gottlober et al. 2003; Zhao et al. 2003a, 2003b; Hatton et al. 2003; Reed et al. 2003; Klypin et al. 2003; Percival et al. 2003; Tasitsiomi et al. 2004; Yahagi, Nagashima, & Yoshii 2004; Gao et al. 2004b), more detailed re-simulations of objects selected from these volumes to determine the structure of individual haloes for reasonably large samples (e.g. Klypin et al. 2001; Jing & Suto 2002; Fukushima & Makino 2001, 2003; Ascasibar et al. 2003; Hayashi et al. 2003; Fukushima, Kawai & Makino 2004; Hoefft, Muckert, & Gottlober 2004; Navarro et al. 2004; Tasitsiomi et al. 2004), and finally very high-resolution simulations of individual haloes focusing on their structure and substructure, either on cluster scales (e.g. Tormen 1997; Tormen, Diaferio & Syer 1998; Ghigna et al. 1998; Coln et al. 1999; Klypin 1999a; Okamoto & Habe 1999; Ghigna et al. 2000; Springel et al. 2001; Goumert, et al.

? PPARC Fellow

email: jet@astro.ox.ac.uk

Ghigna & Moore 2001; De Lucia et al. 2004; Gill, Knebe, & Gibson 2004a; Gillet et al. 2004b; Gao et al. 2004a), on galaxy scales (e.g. Klypin et al. 1999b; Moore et al. 1999a, 1999b; Stoehrer et al. 2002; Power et al. 2003), or both (e.g. Diemand et al. 2004c; Gao et al. 2004b; Weller, Ostriker & Bode 2004; Reed et al. 2004).

This approach has provided a detailed picture of the structure and dynamics of dark-matter-dominated systems over a wide range of scales, from tens of kiloparsecs to hundreds of Megaparsecs. There is a hard limit to the dynamic range that can be achieved using a multi-scale approach, however. Structure formation mixes information on many different scales as haloes form. To model the formation of a halo accurately, one needs to include the effects of very long-wavelength fluctuations together with the smaller fluctuations that produce substructure. Thus the minimum scale that can be included in any self-consistent simulation of a present-day halo is constrained by the requirement that the total volume studied still be in the linear regime (where the effect of larger fluctuations can be accounted for) at the present day, and by the finite numerical resolution available computationally. For the highest-resolution simulations possible currently, this leads to a minimum mass scale for resolved substructure of around  $10^{-4}$  ( $10^{-5}$  of the mass of the main halo considered). To study halo substructure below this mass limit requires analytic or semi-analytic extensions to the numerical results. It is precisely this sort of small-scale information, however, that is required in many current applications including galaxy dynamics, strong lensing, direct or indirect dark matter detection or tests of dark matter physics in general.

In earlier work (Taylor & Babul 2001, TB01 hereafter), we developed a model for dynamical evolution of satellites orbiting in the potential of larger systems. This model includes dynamical friction, tidal mass loss and tidal disruption as its main components. It calculates satellite evolution over a many short time steps, rather like a restricted  $N$ -body simulation, but uses only global properties of the satellite to determine its evolution, thus reducing the computational expense considerably. More recently (Taylor & Babul 2004a, paper I hereafter), we applied this model of satellite evolution to the merging subcomponents involved in the hierarchical formation of galaxy, group or cluster haloes. As one of the main results of paper I, we established a non-parametric way to include realistic amounts of substructure in semi-analytic merger trees without increasing the computational cost substantially. This ‘pruning’ method, together with established merger tree methods and the analytic model of satellite dynamics from TB01, constitute a new semi-analytic model for the formation of individual dark matter haloes.

In this paper, we discuss the basic predictions of this model. In section 2, we first review the model, which was described fully in paper I. In section 3, we then discuss the distribution functions for the mass, peak circular velocity, and spatial location of subhaloes that it predicts. In section 4, we show that these results are relatively insensitive to specific model parameters, uncertainties or assumptions. The model predicts strong correlations among the different properties of subhaloes, and between the age of subhaloes and their other properties, which are discussed in section 5. In section 6, we show how the systematic dependence of subhalo properties on age may allow the use of substructure as

an indicator of the dynamical history of an individual system. Finally in section 7, we consider kinematic grouping of substructure due to the merger sequence, and the effects of encounters between subhaloes. We discuss our results in section 8.

In a subsequent paper (Taylor & Babul 2004b, paper III hereafter) we will compare the predictions of this semi-analytic model with the results of self-consistent numerical simulations of halo formation. This comparison is particularly interesting, since the only free parameters in the semi-analytic model were fixed in paper I, either by matching restricted simulations of individual subhaloes (to fix the parameters of the dynamical model), or by assuming self-similarity in the merging process (to fix the one parameter in the pruning method). Thus we have no remaining parametric freedom when comparing our results to self-consistent simulations, making the comparison a meaningful one.

Finally, we note that as in paper I, here and in paper III we will generally consider results for the former ‘standard’ CDM (SCDM) cosmology with  $h = 0.5$  and  $\Omega_8 = 0.7$ , because the simulations we compare to directly in paper III assumed this cosmology. As illustrated in section 4.2, the properties of substructure depend only weakly on cosmology, and thus we expect our main results to be equally valid for CDM or similar cosmologies. We will consider the cosmological dependence of our results in more detail in future work.

## 2 REVIEW OF THE SEMI-ANALYTIC MODEL

In paper I, we described a full semi-analytic model for studying the formation of dark matter haloes and the evolution of their substructure. In this section we will review briefly the main features of this model. The semi-analytic model consists of several components: a method for generating merger trees, an algorithm for ‘pruning’ these trees, to determine how many distinct satellites merge into the main system within the tree, and an analytic model to describe the subsequent evolution of these satellites.

The merger tree method is an implementation of the algorithm proposed by Somerville and Kolatt (1999). It decomposes a present-day halo into its progenitors at earlier times, using small time steps in order to preserve Press-Schechter (Press & Schechter 1974) statistics. The merger trees considered in this paper generally have a total mass of  $1.6 \times 10^{12} M_\odot$  at  $z = 0$  and a mass resolution of  $5 \times 10^7 M_\odot$ , chosen to match the simulations described in paper III; below this resolution limit they become increasingly incomplete. The merger tree is traced back until all branches drop below the mass resolution limit or a redshift of 30 is reached, and typically contains tens of thousands of branchings.

Within each tree, we can define a main ‘trunk’ by tracing the merger history of the final system back from the present day, choosing the most massive progenitor every time the tree branches, and following this object back in redshift. We will also refer to this as the ‘main system’ or the ‘main halo’ in the tree. We will describe branches off the main trunk as ‘first-order mergers’, branches off these branches as ‘second-order mergers’, and so on. To avoid the computational cost of following the evolution of each sub-branch in the tree, we consider in detail only those systems

that merge with the main trunk of the tree. To treat higher-order branches, we use a simplified description of satellite dynamics to ‘prune’ the merger tree, as described in paper I. We assume that the dynamical age of a satellite, or more specifically the number of orbits it has spent in a system, determines whether it is loosely bound and should be treated as a distinct object when its parent merges with a larger halo, or whether it is tightly bound and should be considered part of its parent. By self-similarity, we established in paper I that the average time delay separating the two cases should be  $n_0 \approx 2.0$  (2.2 orbital periods, depending on the disruption criterion assumed). Thus if higher-order substructure has spent more than 2 orbits in its parent halo when that parent merges with a lower-order branch, then we treat it as part of its parent. Otherwise, we treat it as a distinct merger with the lower-order system.

As a satellite evolves in a parent’s halo, it also loses mass. From self-similarity, we determined in paper I that satellites that had spent  $n_0$  orbital periods or less in their parent system retained an average fraction  $f_{st} = 0.73$  of their original mass. Thus if a satellite of mass  $M_s$  has spent less than  $n_0$  orbits in its parent’s halo, it is passed on to the next lower-order system with a mass  $0.73 M_s$ , while the remaining mass is added to its original parent. In the full merger tree, satellites of initial order  $n$  will thus be reduced to  $(f_{st})^{(n-1)}$  of their original mass when they finally merge with the main trunk. (Here and in what follows, the ‘original mass’  $M_{s,0}$  is the mass a subhalo has before it merges with a larger system for the first time, while the ‘infall mass’  $M_{s,i}$  is the mass a subhalo has when it merges with the main trunk.)

Using this ‘pruning’ method, we determine how much substructure percolates down to the main trunk of the merger tree. After being pruned in this way, a typical merger tree contains roughly 4000 branches, each recording the merger of a single satellite with the main system. If these satellites were part of the same branch before pruning, we consider them to be part of the same kinematic group, and give them correlated initial orbits, as described in paper I. Otherwise they are distributed on randomly oriented orbits starting at the virial radius, with a realistic distribution of angular momenta. The only other property we need to specify for the subhaloes is their initial density profile, which is assumed to be a Moore profile,  $\rho(r) = \rho_0 r^{-1.5} = (r_s^{-1.5} + r^{-1.5})$ . Although the most recent high-resolution simulations (Power et al. 2003; Fukushige, Kawai & Makino 2003; Navarro et al. 2004; Tasitsiemi et al. 2004; Diemand et al. 2004b) suggest that typical haloes have a central density profile with a slope closer to the value of  $-1$  suggested by Navarro, Frenk and White (1996, 1997, NFW hereafter), the Moore fit gives a better representation of the excess central mass, relative to the NFW fit, seen in the simulated haloes.

The subhalo profiles can also be reparameterised in terms of their original virial radius  $r_{vir}^{-1}$  and their concentration  $c = r_{vir}/r_s$ . Since the virial radius of a halo depends only on its total mass and on the background cosmology, iso-

lated spherical haloes of a given mass at a given redshift are completely specified by their concentration. We determine concentrations by applying the relations of Eke, Navarro and Steinmetz (2001, ENS01 hereafter) to each system at the time it first appears in the merger tree, that is the last time it is an independent object, as opposed to substructure in a larger system. (We divide the ENS01 concentration by a factor  $r_{s,N}/r_{s,M} = 1.73$ , to account for the relative difference in scale radius between the Moore and NFW profiles, as explained in paper I.) If the subhalo is stripped before falling into the main system, its density profile is modified according to the formula proposed in Hayashi et al. (2003, H03 hereafter; equation 8), specifically:

$$\rho(r) = \frac{f_c}{1 + (r/r_c)^3} \rho_0(r); \quad (1)$$

where  $\rho_0$  is the original density profile,  $f_c$  describes the reduction in central density as the system is stripped, and  $r_c$  indicates the radius beyond which the system is almost completely stripped by tides. Formulae relating  $f_c$ ,  $r_c$  and the declining peak circular velocity to the net amount of mass loss are given in H03 (see their Fig. 12).

The subsequent evolution of the individual subhaloes is determined using the analytic model of TB01 to account for dynamical friction, mass loss, tidal heating and disruption. The evolution of the density profile as mass is lost is described in H03. There is some uncertainty as to when satellites will be completely disrupted by repeated mass loss. As discussed in paper I, we consider satellites disrupted if they are stripped down to a critical fraction of their mass,  $f_{dis}$ , corresponding to the mass within either 0.5 or 0.1 times the binding radius defined by H03. (For the satellites considered here this is equivalent to 2.4 percent or 0.24 percent of the original mass, respectively.) In what follows, we will refer to these two cases as models ‘A’ and ‘B’. Satellites are also considered disrupted if they enter into the central  $0.01 r_{vir,M}$  of the main halo, since we expect mass loss to be rapid in this region, but we cannot follow satellite evolution accurately this far into the potential without using much shorter time steps than are required for the rest of the tree.

The basic properties of the main system, specifically its mass and virial radius at a given redshift, are also determined directly from the merger tree. We assume unless specified otherwise that the main system has a Moore density profile, and a concentration or scale radius given by the relations in ENS01. Our fiducial system, a  $1.6 \times 10^{12} M_\odot$  halo at  $z = 0$  in a  $\Lambda$ CDM cosmology, has a concentration  $q_M = 10.3$ , a scale radius  $r_{s,M} = 30.5$  kpc, a virial radius  $r_{vir,M} = 314.1$  kpc, and a virial velocity (or circular velocity at the virial radius)  $v_{vir} = 148$  km s $^{-1}$ . We note that this concentration is typical for a galaxy of this mass (ENS01); galaxy clusters would be about half as concentrated, so one must keep this difference in mind when comparing our results with simulations of more massive systems. On the other hand, real galaxy haloes have large concentrations of baryonic material at their centres, and through adiabatic contraction they may have become more concentrated than the systems considered here; this possible difference should be kept in mind when comparing with observations.

In all, the dynamical model has two main free parameters: the Coulomb logarithm  $\ln \Lambda$  which modulates dynamical friction, and the heating coefficient  $\eta$  which modulates

<sup>1</sup> We will use the standard definition of  $r_{vir}$  derived from the spherical collapse model, as the radius within which an isolated halo has a mean density  $\rho_{vir}$  that exceeds the critical density  $\rho_c$  by a factor  $\Delta_c$  which depends on cosmology.

## 4 Taylor & Babul

mass loss. (A third parameter discussed in TB01, the disk logarithmic  $f_{\text{dis}}$ , is not used here since we are considering evolution in a single-component potential). The precise disruption criterion (say the fraction of the binding radius used to define  $f_{\text{dis}}$ ), the form chosen for the density profile of the satellites and the profile of the main system, and various other model choices will also affect some of our results, though not very strongly. We will discuss the model dependence of our results in section 4. We first present results for the default parameter values discussed in paper I, specifically  $\alpha_s = 2.4$  (where the magnitude of dynamical friction scales as  $\langle M \rangle = \alpha_s + \ln(M_h/140M_s)$  if  $m < M = 140$ , and  $\langle M \rangle = \alpha_s$  for  $m \geq M = 140$ ), and  $\alpha_h = 3.0$ . The disruption criterion assumes either  $f_{\text{dis}} = 0.5$  (model A) or  $f_{\text{dis}} = 0.1$  (model B). Given these parameter choices, the pruning parameters are fixed iteratively as discussed in paper I. For model A  $n_o = 2.0$ , and for model B  $n_o = 2.2$ , while  $f_{\text{st}} = 0.73$  in both cases.

### 3 BASIC PREDICTIONS FOR HALO SUBSTRUCTURE AT $z = 0$

#### 3.1 Cumulative distributions and higher moments

The first high-resolution simulations of galaxy haloes (Klypin et al. 1999b; Moore et al. 1999a) demonstrated that halo substructure is very close to self-similar across a wide range of halo mass and for different CDM cosmologies. In particular, the cumulative number of subhaloes with internal circular velocities equal to a given fraction  $f$  of the velocity of the main halo, as a function of  $f$ , is roughly universal. A number of other simulations (e.g. Okamoto & Habe 1999; Springel et al. 2001; Governato et al. 2001; Stoehr et al. 2002; Desai et al. 2004; Reed et al. 2004; De Lucia et al. 2004; Gao et al. 2004b; Weller et al. 2004) have confirmed the universal form for the cumulative distribution of relative circular velocity (or ‘cumulative relative velocity function’), and have shown that the cumulative relative mass function is also roughly universal. Thus we will quantify the predictions of the semi-analytic model in terms of these cumulative functions  $N(>v_p)$  and  $N(>M)$ , as well as the higher-order dependence of these functions on position within the halo. We re-examine the universality of the cumulative functions derived from numerical simulations in paper III.

##### 3.1.1 $N(>M)$

Although there are different conventions for determining the total mass of a halo or subhalo, they yield similar values, and therefore the normalisation of the cumulative mass function is straightforward. We choose the convention of normalising subhalo masses (denoted  $M_s$ ) to the virial mass of the main system predicted by the merger tree model at the redshift considered (normally  $z = 0$ ),  $M_{\text{vir},m}$ . As explained in paper I, this is the mass within a region of mean density  $\bar{\rho}_c$  at that redshift. Since our fiducial mass  $1.6 \times 10^{12} M_\odot$  is a reasonable estimate for the total virialised mass surrounding a system like the Milky Way at  $z = 0$ , we will also indicate the absolute values of subhalo masses, to facilitate comparison with the satellites of the Milky Way. We will discuss the normalisation of the numerical results in section paper III.

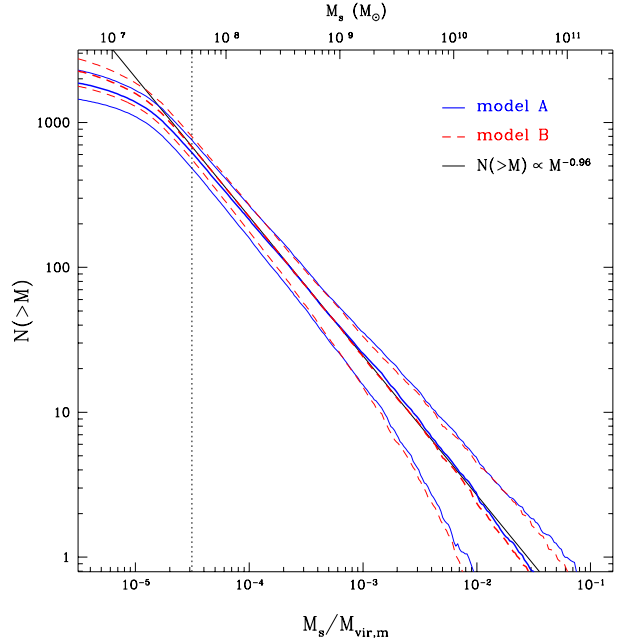


Figure 1. The cumulative mass functions predicted by the semi-analytic model. The thick lines show the average result for a 104 SCDM merger trees at  $z = 0$ , for model A (solid lines) and model B (dashed lines). The thin lines show the 1- $\sigma$  halo-to-halo scatter. The thin solid line shows a power-law of slope  $-0.96$ , while the vertical line indicates the mass resolution limit of the original merger trees.

Fig. 1 shows the cumulative relative mass functions predicted by the semi-analytic model at  $z = 0$ . The thick lines are the mean for a set of 104 trees, and the thin lines indicate the 1- $\sigma$  halo-to-halo scatter. (Solid lines are for model A and dashed lines are for model B.) The top axis indicates the corresponding subhalo mass in a system with a virial mass of  $1.6 \times 10^{12} M_\odot$ . Over the range resolved by the merger trees ( $M_s > 5 \times 10^7 M_\odot$ ), the cumulative mass function is very close to a power law:  $N(>M) = N_0 (M_s/M_{\text{vir},m})^{-\alpha}$ , with  $N_0 = 0.038$  and  $\alpha = 0.93$  for model A and  $N_0 = 0.032$  and  $\alpha = 0.96$  for model B (this fit is included as a thin solid line on the plot). The 1- $\sigma$  halo-to-halo scatter is approximately 20–30 percent at the low mass end, but more than a factor of two at the high mass end.

##### 3.1.2 $N(>v_p)$

The normalisation of velocities is more problematic. Two different velocities, the virial velocity (or circular velocity at the virial radius)  $v_{\text{vir}} = \sqrt{GM_{\text{vir}}/r_{\text{vir}}}$ , and the velocity at the peak of the rotation curve  $v_p$ , can be used to characterise an isolated halo<sup>2</sup>. Subhaloes within a larger system will be tidally truncated, so the equivalent of the virial velocity in these systems will be the circular velocity at some outer radius that marks their tidal limit. In order to compare our the properties of subhaloes to simulations, we will consider

<sup>2</sup> For an NFW profile of concentration  $c$ , the ratio  $v_p/v_{\text{vir}} = 0.465 [\ln(1+c)/c - 1/(1+c)]^{0.5}$ . The approximation  $v_p/v_{\text{vir}} = 1.0 + 0.025(c - 2.163)$  holds to better than 2 percent for  $c = 2\{20$ , the typical range for galaxy and cluster haloes.

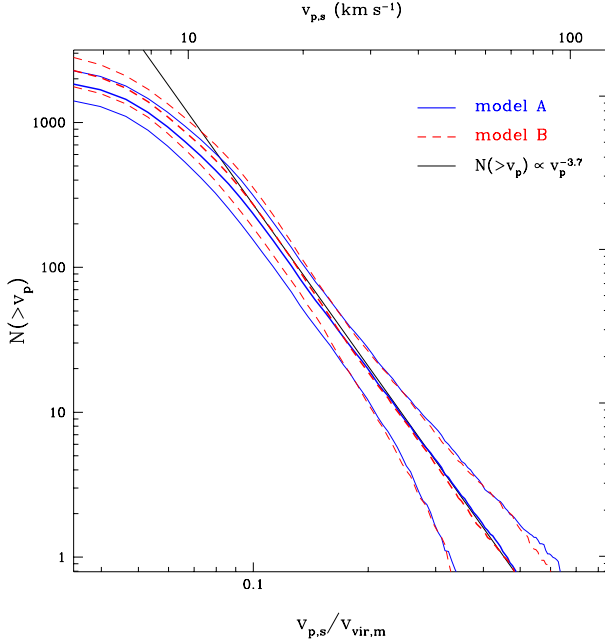


Figure 2. The cumulative peak circular velocity functions predicted by the semi-analytic model. The thick lines show the average result for a 104 SCDM merger trees at  $z = 0$ , for model A (solid lines) and model B (dashed lines). The thin lines show the 1- $\sigma$  halo-to-halo scatter. The thin solid line shows a power-law of slope  $-3.7$ .

the peak velocity  $v_p$ , as it is easier to measure reliably in simulations, whereas the outer radius of a system may be poorly determined. On the other hand, the peak velocity has an additional and quite large dependence on the concentration of the system. Thus, we will normalise subhalo velocities to the virial velocity of the main system (denoted  $v_{vir,m}$ ) rather than its peak velocity when comparing results for different haloes, and plot distributions in terms of the velocity ratio  $v_{p,s}/v_{vir,m}$ .

Fig. 2 shows the cumulative relative velocity function predicted by our model at  $z = 0$ , that is the cumulative distribution of peak circular velocity  $v_{p,s}$ , relative to the virial velocity  $v_{vir,m}$  of the main system. Line styles are as in Fig. 1, and as before the top axis indicates the corresponding peak velocities of subhaloes in a system with a virial velocity of  $148 \text{ km s}^{-1}$ . In the range resolved by the merger trees ( $v_{p,s} > 10 \text{ km s}^{-1}$ ), the cumulative velocity function is close to a power law:  $N(>v_{p,s}) = N_0 (v_{p,s}/v_{vir,m})^\alpha$ , with  $N_0 = 0.07$  and  $\alpha = 3.5$  for model A and  $N_0 = 0.054$  and  $\alpha = 3.7$  for model B (this is included as a thin solid line on the plot). We note that if all subhaloes had peak velocities proportional to their original virial velocities, we would expect a slope  $\alpha = 3$ . The actual slope is steeper due to the concentration-mass-redshift relation, which implies that low-velocity systems are more concentrated on average, and thus that have higher values of  $v_p/v_{vir}$  initially. Finally, we note that as with the mass function, the 1- $\sigma$  halo-to-halo scatter in the velocity function is 20/30 percent at the low velocity end, but more than a factor of two at the high-velocity end.

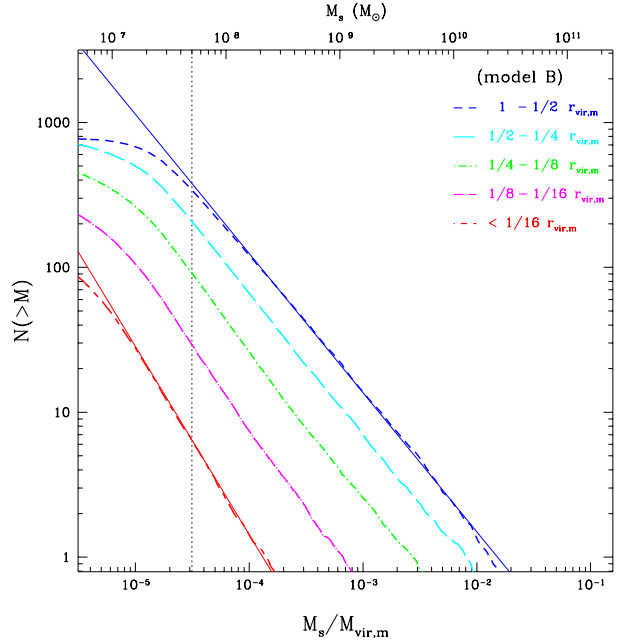


Figure 3. The cumulative mass function of subhaloes in different radial bins, for haloes generated using model B. The slope of the mass function varies from  $\alpha = 0.96$  in the outermost radial bin to  $\alpha = 1.3$  in the innermost bin, as indicated by the thin lines.

### 3.1.3 $N(M < R)$

We expect the mass and circular velocity of a subhalo to be correlated with its position within the main halo. This is both because subhaloes close to the centre of the main system will have merged with the main system at a higher redshifts on average, and also because they will have lost more mass through tidal stripping. Fig. 3 shows how the cumulative mass function varies, when binned in radius. In the outer parts of the halo, it has essentially the same slope as the mass function for the whole halo,  $\alpha = 0.96$ . In the innermost regions, the slope steepens, so that within  $r < r_{vir,m}/16$  ( $\approx 20 \text{ kpc}$  in our fiducial system),  $\alpha = 1.3$ . Since the differential mass function goes as  $dN/dM \propto M^{-1}$ , and the contribution to the mass from substructure of mass  $M$  or greater goes as  $f(>M)/M^{(1)+1} = M^{-1}$ , a slope of  $\alpha < 1$  implies that this quantity will diverge as we integrate down to smaller and smaller masses. Thus, the question of how much of the dark matter at the centres of haloes is in bound substructure remains highly uncertain. This uncertainty has important implications for attempts to detect dark matter observationally or experimentally, as discussed in paper III.

### 3.1.4 $N(R < R_{km})$ , $N(R < R_{kv_p})$

We can also take other moments of the substructure distribution. Fig. 4 shows the radial number density profile of the subhalo distribution, for subhaloes binned in several different ways. In the top left panel, the different curves all have the same normalisation (they are all multiplied by the volume within the virial radius,  $V_{vir} = 4\pi r_{vir,m}^3/3$ ). In the other panels, the number density in each bin has been normalised to the mean number density within the virial ra-

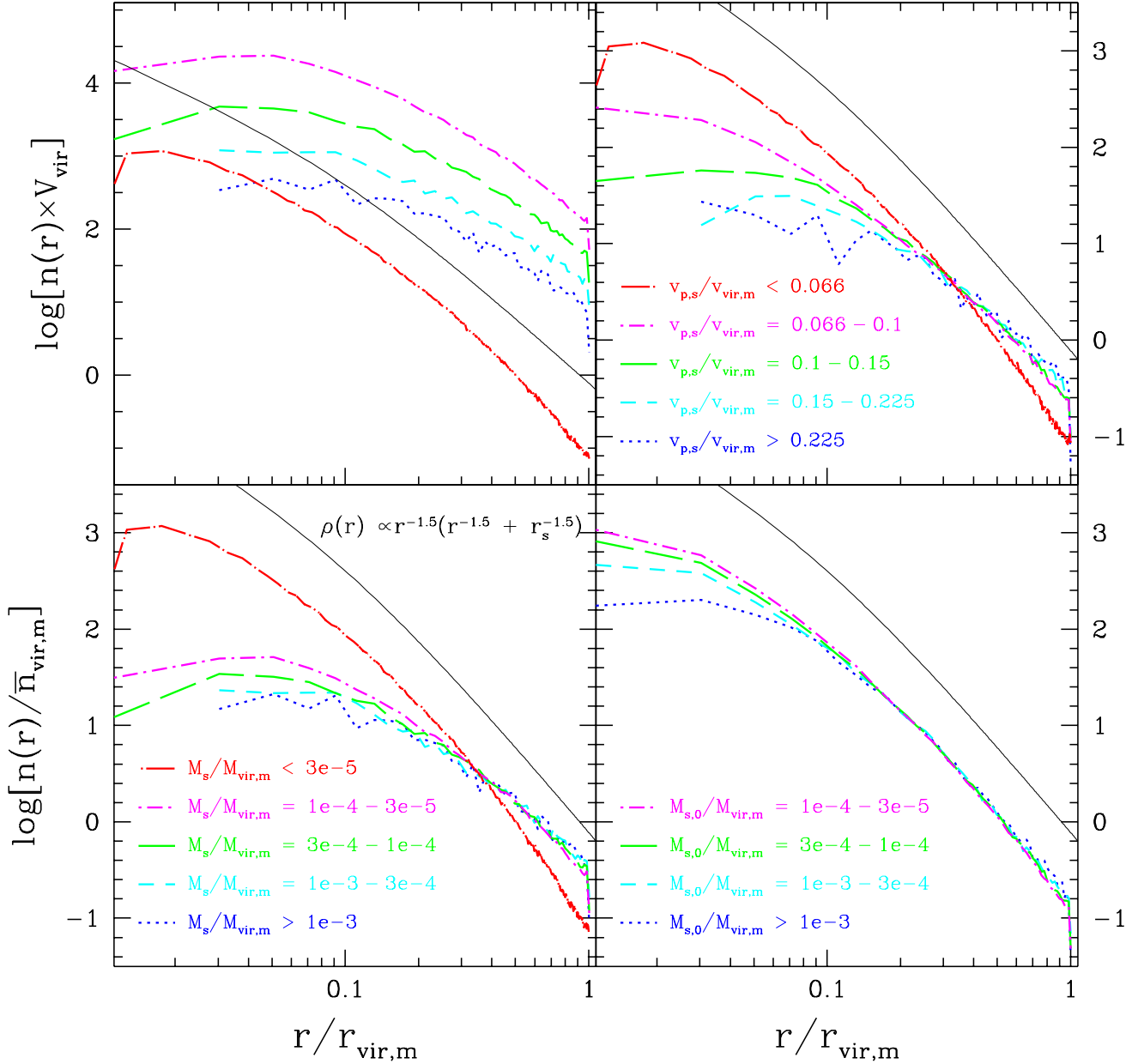


Figure 4. The number density of subhaloes as a function of their position in the main system, binned and normalized in various ways. The top left-hand panel shows the number density multiplied by the virial volume, binned by their mass at  $z = 0$ . The other panels show the number density normalized to the mean within the virial radius for objects in that bin. Systems are binned by their mass at  $z = 0$  (bottom left), their original mass (as defined in the text) (bottom right), and by their peak circular velocity at  $z = 0$  (top right). In each case, only systems that survive at  $z = 0$  are included. The thin lines show a Moore density profile of concentration  $c_M = 10$ , with arbitrary normalization.

radius for objects in that mass range. Systems are binned by their mass at  $z = 0$  (two left-hand panels), their original mass  $m_{s,0}$  defined previously (bottom right panel), and by their peak circular velocity at  $z = 0$  (top right panel). In each case, only systems that survive at  $z = 0$  are included. The thin lines show a Moore density profile of concentration  $c_M = 10$ , with arbitrary normalization.

In the left-hand panels, in the four mass bins above our

resolution limit ( $5 \times 10^7 M_\odot$ , or  $3 \times 10^{-5} M_{\text{vir},m}$ ), the number density profiles are appreciably shallower than the background density profile. They appear to have central cores of roughly constant number density, ranging in size from 5 to 15 percent of the virial radius in size (15/45 kpc in our fiducial system), depending on the mass bin. From the absolute scaling in the top left-hand panel, it is clear that the total distribution summing over the four bins above the resolution

limit will be dominated by the subhaloes in the lowest mass bin, and will therefore have a profile similar to the lower dot-dashed line. Given the steepness of the subhalo mass function, this will always be the case for number-weighted distributions, and thus the radial distributions determined in simulations will depend on the limiting mass resolution and the completeness near that limit. This may be one reason why different methods for identifying substructure can determine quite different radial distributions for the same simulation (Gill et al. 2004a, Fig. 9).

Objects in the mass bin below the resolution limit have a radial distribution that is even more centrally concentrated than the background density profile. This result is mainly due to the incompleteness of the merger tree at these masses, however. Given our initial mass resolution, the systems in this bin must have lost some mass, and most will have lost a large fraction of their mass. This explains why they are preferentially found in the central part of the halo where mass loss rates are higher. Extending the merger tree completely down to this mass range would reveal more low-mass systems in the outer part of the halo, producing a shallower profile. Overall, the trend in the radial distributions above the mass resolution limit suggest that the subhalo distribution will approach the background mass distribution as the resolution limit decreases. The convergence to this final profile may be very slow, however, as discussed in paper III.

The two right-hand panels show the normalised distributions of subhaloes binned in various other ways. The top right-hand panel shows the normalised distribution of systems binned by present-day peak circular velocity, since this may be more relevant in comparisons with observational data (Nagai & Kravtsov 2004). Unfortunately the resolution limit of the tree is not defined precisely in this variable, so all the bins below  $v_{p,s} = v_{vir,m} / 0.1$  are affected to some degree by the incompleteness of the merger tree. Otherwise, the general trends are as in the bottom left-hand panel.

The bottom right-hand panel shows all surviving systems binned in terms of their original mass. Down to  $0.1 r_{vir,m}$ , there is very little difference in the results as a function of mass. This agrees with the numerical results of Nagai & Kravtsov (2004), who found that there is little variation in the radial distribution of subhaloes as a function of their mass at the time of accretion onto the main halo. The overall distribution matches the mass distribution of the main system very closely, as found by Nagai & Kravtsov (2004) and Gao et al. (2004), who used semi-analytic galaxies to trace the distribution of stripped haloes in their cluster simulations. In the innermost regions of the halo, we do find fewer surviving remnants of massive subhaloes, relative to less massive subhaloes. This is partly because the subhaloes in these regions are older, and the average mass scale of substructure was smaller at earlier times, but it is also because dynamical friction has caused many of the more massive central systems to fall in to the centre of the potential and be disrupted.

## 4 MODEL DEPENDENCE

### 4.1 Dependence on model parameters

Since the relative efficiency of various physical processes is parameterised explicitly in the semi-analytic model, we can

test the sensitivity of our results to the input physics by running the model with different values for these parameters. In particular, we can test how the amplitude of the mass function depends on  $\ln_{\text{h}}$ ,  $\ln_{\text{h}}$  and other parameters in the model. The variation in the results is generally fairly small, so to highlight the differences, we take parameter values at the extremes of, or even beyond, their probable range, and normalise the results for these variant models to the fiducial results from model B.

Fig. 5 shows the amplitude of the (differential) subhalo mass function for different variant models, relative to the mass function in the fiducial model. These are (clockwise from the upper left panel) a) different values for the parameters describing subhalo dynamics, specifically  $\ln_{\text{h}} = 2.0$  rather than 3.0 or  $\ln_{\text{h}} = 24$  rather than 2.4 (model A is also shown for comparison); b) using an NFW density profile for the main halo, using NFW profiles for the subhaloes, or using the concentration relation from Bullock et al. (2001); c) including additional mass loss and disruption due to collisions (see section 7.2); and d) using very circular ( $\Gamma = 0.6$  rather than 0.4) or very radial distributions ( $\Gamma = 0.25$  and  $\Gamma = 0.17$ ) for subhalo orbits, or increasing the initial orbital velocity to  $1.5v_{vir,m}$ . In each case, we divide the variant mass function by the fiducial mass function. The error bars show the approximate level of fluctuations in the fiducial mass function. Note that we have not rerun our full model to determine a consistent pruning condition for each of these variant runs; thus all we show here is how strongly the model parameters affect a given set of subhaloes.

Overall, the mass function appears to be remarkably robust to changes in the model, particularly since we have chosen parameter values that are actually outside the expected range of uncertainty in many cases, in order to produce a clear effect on the mass function. Increasing the strength of dynamical friction reduces the number of massive satellites that survive in the system, but we have had to increase the Coulomb logarithm by a factor often to see a clear difference in the mass function; for realistic values of  $\ln_{\text{h}}$  the effect of any uncertainty in the exact strength of dynamical friction is negligible. This is probably because dynamical friction is relatively ineffective much below  $M_s = M_{vir,m} / 10^2$  (cf. paper I), and the average system has few satellites in this range. Heating has a slightly larger effect; reducing the heating coefficient by 30 percent, a reasonable change given the uncertainty in its value, increases the normalisation of the mass function by roughly 10 percent. The difference between models A and B is also 10–20 percent in amplitude; changing the pruning parameters  $n_o$  or  $M_{st}$  by 10 percent produces a change of similar magnitude, steepening the slope of the mass function as  $n_o$  increases or  $M_{st}$  decreases.

Changing the subhalo density profile to an NFW profile with a shallower central cusp has almost no effect on the mass function (top right-hand panel). If we use the concentration relations of Bullock et al. (2001), small haloes are more concentrated and less sensitive to tidal stripping, increasing the amplitude of the mass function by 20 percent. Changing the profile of the main system has a larger effect however, increasing the amplitude of the mass function by 30 percent. Increasing the concentration of the main halo sufficiently also produces similar results. This demonstrates the importance of the central cusp in stripping and disrupting subhaloes as they pass through the pericentres of their



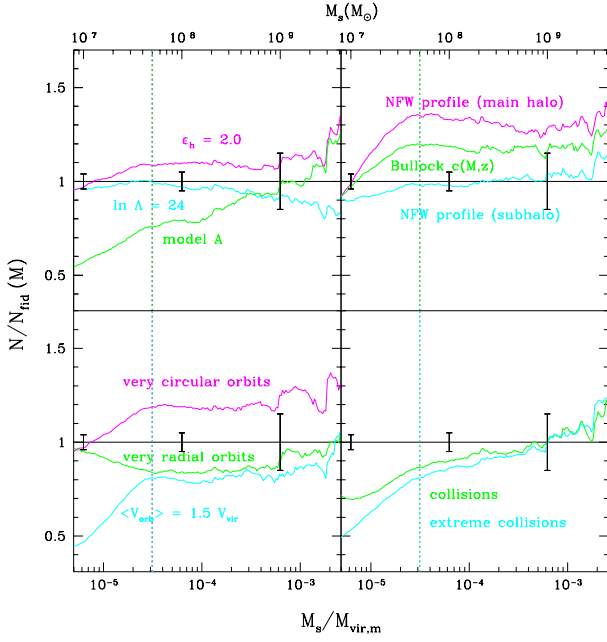


Figure 5. The relative change in the (differential) mass function for trees evolved in different variants of the basic model, including (clockwise from upper left): a) varying the parameters describing subhalo dynamics (model A is also shown for comparison), b) varying the density profiles of the subhaloes or the main halo c) including additional mass loss and disruption due to collisions, or d) varying the distribution of subhalo orbits. In each case, we divide the variant mass function by the fiducial mass function. The error bars show the approximate level of fluctuations in the fiducial mass function. The vertical dotted line indicates the resolution limit of the merger trees; note that many of the mass functions change systematically below this limit due to incompleteness.

orbits. It also implies that adding a central galactic component to the halo may reduce considerably the number of subhaloes of a given mass that survive in the central part of a halo. (We note that the numerical simulations analysed in paper III are dark-matter only, so their lack of central substructure is not be due to the disruptive effects of a central galaxy.)

One process that is not included in our basic model of subhalo dynamics is the effect of collisions and encounters between subhaloes, or ‘harassment’. In section 7.2 we will describe an approximate way of recording collisions and modelling their contribution to mass loss and disruption. The bottom right-hand panel shows that the overall effects predicted by this model are fairly minor, however; the amplitude of the mass function is reduced at intermediate and small masses, but only by 10–15 percent (the overall slope of the mass function also changes systematically, decreasing by about 10 percent). Thus collisions do not seem to offer a plausible way of getting rid of substructure.

Finally, the lower left-hand panel shows the effects of varying subhalo orbits. Increasing the circularity of subhalo orbits (from  $\bar{m} = 0.4$  to  $\bar{m} = 0.6$ ) produces has a reasonably large effect, presumably because it moves their pericentres out of the centre of the system. Khochfar and Burkert recently reported an initial distribution of subhalo orbits from large-scale simulations that was more radial than assumed

here. Although it has since become apparent that the radial bias was due to an unsubtracted contribution from the Hubble flow (Khochfar and Burkert 2003; Benson 2004), we can nonetheless test what effect this sort of distribution would have on our results. To match the distribution of circularities they first reported, we take a Gaussian distribution with  $\bar{m} = 0.25$  and  $\sigma = 0.17$ . This results in a 15 percent reduction in the amplitude of the mass function. Finally, the third curve in this panel shows the effect of varying initial subhalo velocities. The theoretical uncertainty in this quantity turns out to be less important, as even an unrealistically large change (increasing the mean velocity by 50 percent, or more than doubling the mean kinetic energy) produces only a 20 percent reduction in the amplitude of the mass function.

In summary, testing our model for sensitivity to uncertainties in its different components, we find that variations in the model parameters over a plausible range have only a minor effect on the subhalo mass function. In particular, given reasonable variations in the parameters, the mass function is very insensitive to the exact magnitude of dynamical friction, the central slope of the subhalo density profile, or to minor collisions. It is mildly sensitive (varying by 10–15 percent for reasonable variations in the parameters) to subhalo concentrations, more radial subhalo orbits, larger subhalo velocities or strong collisions. Only changing the central density profile of the main halo or placing subhaloes on very circular orbits has a large (20–30 percent) effect on the mass function. This is consistent with the general conclusion from paper I that a subhalo’s properties are strongly affected by the density of the main system at the pericentre of its orbit, through friction, stripping, and disruption. Other subhalo properties, such as their spatial distribution, may also vary systematically with the input parameters. We discuss this variation in section paper III.

#### 4.2 Dependence on cosmology

In most of this paper, we will present results generated in an  $\Lambda$ CDM cosmology, in order to compare them with earlier numerical work which assumed this cosmology. There are now much stronger observational constraints on the cosmological parameters; in particular, combining WMAP observations with other data sets gives extremely strong evidence for non-zero cosmological constant. We have rerun our trees for a  $\Lambda$ CDM cosmology with  $\Omega_m = 0.3$ ,  $h = 0.7$  and  $\Omega_\Lambda = 0.7$ , a choice of parameters roughly consistent with the analysis of the first year of WMAP data. After appropriate scaling, we find substructure very similar to that in the  $\Lambda$ CDM halos. Fig. 6, for instance, shows that the average cumulative mass function in  $\Lambda$ CDM haloes is very similar to the  $\Lambda$ CDM mass function, although with 10–20 percent fewer objects at the highest and lowest masses. The slightly reduced amplitude of the mass function is consistent with numerical  $\Lambda$ CDM mass functions (e.g. Springel et al. 2001; Font et al. 2001; Governato et al. 2001; Stoehr et al. 2002; Desai et al. 2004; Reed et al. 2004; De Lucia et al. 2004; Gao et al. 2004b; Weller et al. 2004). A test to the slope of the  $\Lambda$ CDM mass function in the mass range  $M_s = M_{vir,m} = 10^{-3}$  to  $10^{-4}$  gives  $\alpha = (0.9) \pm (0.02)$ .

Perhaps more importantly for our method, the pruning parameters (which we determine by requiring self-consistency (see paper I) derived for the  $\Lambda$ CDM trees



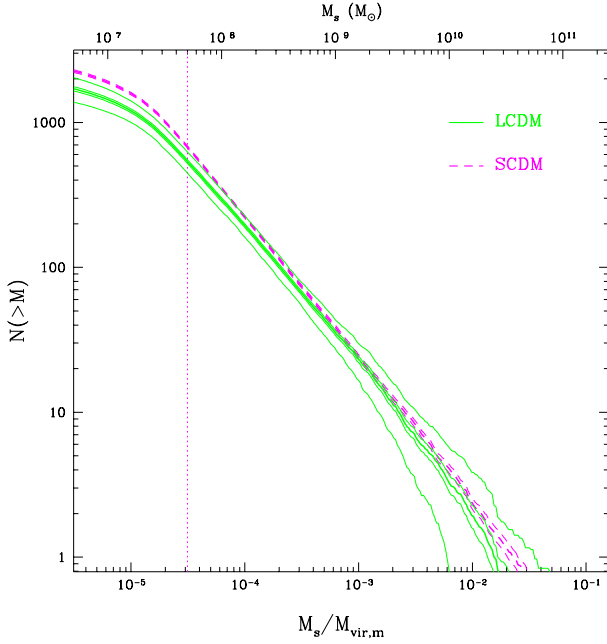


Figure 6. The average cumulative mass function for LCDM subhalos (thick solid line, with thin lines indicating the 1- $\sigma$  uncertainty in the mean and the 1- $\sigma$  halo-to-halo scatter), compared with the SCDM mass function (dotted lines, with upper and lower lines showing the 1- $\sigma$  uncertainty in the mean).

are very similar to those in the SCDM trees (we find  $\bar{M} = 0.365$ ,  $f_{\text{st}} = 0.725$ , and  $n_o = 2.3$  for model B in LCDM, versus  $\bar{M} = 0.335$ ,  $f_{\text{st}} = 0.677$ , and  $n_o = 2.25$  for model B in SCDM). This is encouraging, as it suggests the pruning parameters required for self-consistency are fairly insensitive to the precise cosmology. We will re-examine the dependence of halo substructure on cosmological parameters in more detail in future work.

## 5 EVOLUTION OF SUBHALO POPULATIONS WITH TIME

In the previous section, we considered the properties of halo substructure at the present-day, averaging over systems with very different dynamical histories. The properties of individual subhalos will change systematically as they evolve within a larger system, however, and thus the average properties of substructure in a halo will depend on its dynamical age and assembly history. In this section, we review how subhalo properties change with time, we show how this dependence produces correlations between position, mass and subhalo properties, and we quantify the relation between the assembly history of a halo and the mean properties of its substructure.

### 5.1 Properties of individual subhaloes as a function of their age

To characterise the age of each subhalo merging with the main system we can define two different epochs within the merger tree, as discussed in paper I; the ‘merger epoch’  $z_m$  when a subhalo merges with the main trunk of the tree (that

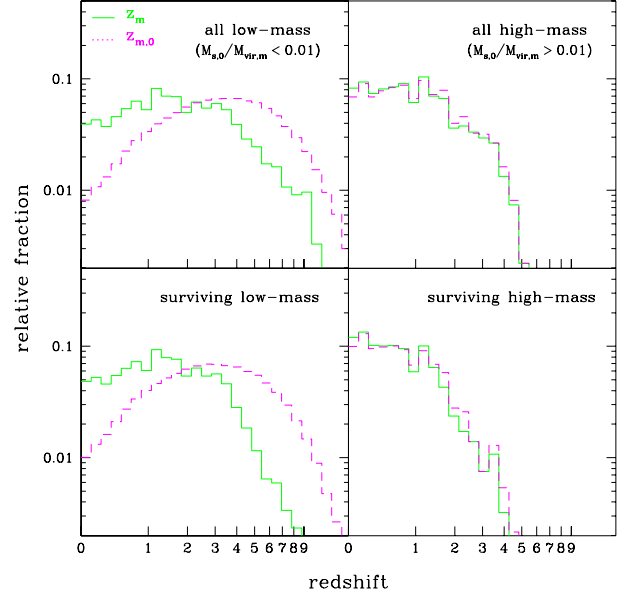


Figure 7. Histograms of the merger epoch (solid line) and the original epoch at which systems first appeared in the merger tree (dashed line), for all subhalos (top panel), and for those subhalos that survive to the present-day, in model B. Left and right-hand panels are for low and high mass systems respectively.

is the main progenitor of the final system), and the ‘original merger epoch’  $z_{m,0}$  at which it last exists as a distinct entity within the merger tree. (These two redshifts are indicated schematically in Fig. 17 of paper I.) The original merger epoch  $z_{m,0}$  will be greater than  $z_m$  if the subhalo merges with another system before falling into the main system, that is to say if it is a ‘higher-order’ subhalo in the sense defined in section 2. The original merger epoch is particularly important as it determines the original density profile of the subhalo, before it is modified by tidal stripping in subsequent mergers.

Fig. 7 shows the distribution of these two redshifts for subhalos in model B, divided up according to their mass when they first merge with the main halo (left and right panels corresponding to systems with original masses less than or greater than 1 percent of the present-day mass of the main halo, respectively) and whether they survive to the present-day. Most high-mass subhalos have merged into the main system since redshift 1.2, while low-mass subhalos have typical merger epochs of 1.4. For massive subhalos,  $z_{m,0}$  is usually equal to  $z_m$ , since most of these systems merge directly with the main system. On the other hand the low-mass subhalos are often higher-order systems, and as a result the distribution of  $z_{m,0}$  extends back to much higher redshift.

Recent numerical studies of halo substructure at very high resolution have found similar results. Fig. 10 of De Lucia et al. (2004), for instance, shows results comparable to the lower right-hand panel (albeit for more massive haloes in a  $\Lambda$ CDM cosmology), while Fig. 12 of Gao et al. (2004b) shows similar results for cluster, group and galaxy haloes. In general, we predict more old substructure than is seen in these simulations. In model B, about 30 percent of surviving massive subhalos merged before  $z = 1$ , whereas Gao et al.

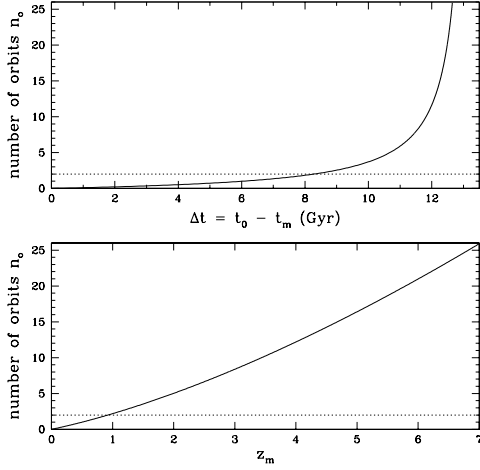


Figure 8. The number of orbits (i.e. pericentric passages) a typical satellite has completed, as a function of the time it has spent in the main system  $n_o = t_0 - t_m$  (top panel) or the merger epoch  $z_m$  (bottom panel).

and only 10 percent of their surviving systems are this old. We will discuss this discrepancy further in paper III.

In paper I we also introduced the quantity  $n_o = P_{\text{rad}}$ , the time a subhalo has spent in the main system in units of the radial period at the virial radius of the main system at the time the subhalo first fell in<sup>3</sup>, as an estimate of how many pericentric passages it has undergone (pericentric passages occurring at  $n_o = 0.25(0.5)$ , and once per radial period thereafter). Since the radial period  $P_{\text{rad}}$  depends in a simple way on  $z_m$ , there is a straightforward relation between  $n_o$  and  $z_m$ , as illustrated in Fig. 8. In particular, for the SCDM cosmology considered here,  $P_{\text{rad}} \approx 0.835 t_m$ , where  $t_m$  is the age of the universe at redshift  $z_m$ , and the numerical factor depends slightly on the density profile of the main system. Thus  $n_o = (t_0 - t_m) / P_{\text{rad}} \approx (t_0 - t_m) / 0.835 t_m \approx 1.2(t_0/t_m - 1)$ , where  $t_0$  is the present age of the universe.

Subhalo properties will depend on merger epoch for several reasons:

As the main system grows its satellite population extends to progressively larger masses.

As the main halo grows its virial radius increases, and satellite orbits become correspondingly larger.

The central densities and mean densities of infalling satellites decrease with time, according to the EPS merger model and the concentration-mass-redshift relation for haloes.

The density profile of the main system changes with time, although in practice this change is mainly confined to the outer parts of the halo.

Subhaloes will be stripped and disrupted with time, so the properties of the surviving population will depend on how long they have spent in the main system.

Fig. 9 shows the net effect of all these terms on subhalo properties. The upper left-hand panel shows the aver-

age fraction of their infall mass that subhaloes have retained as a function of merger epoch. The thick lines show the mean value in each bin in merger epoch, for model A (solid line) and model B (dashed line), while the dotted lines show the 1- $\sigma$  scatter in each bin. The overall behaviour is similar for both models; the mean value of  $M/M_0$  decreases rapidly back to  $z_m = 2$ , and is roughly constant at higher redshifts, although the scatter around the mean remains large, due to different subhalo orbits, masses and densities.

The top right-hand panel shows how the fraction of surviving subhaloes decreases as a function of  $z_m$  (thick solid and dashed lines for models A and B respectively), while the fraction of disrupted subhaloes (thin solid or dashed lines) or of subhaloes that have fallen into the centre of the main halo (solid triangles or open squares, for models A and B respectively) increases progressively.

We can compare these results with the numerical results of Gao et al. (2004b, Fig. 14). In simulated clusters, their group finder can locate 40{55 percent of all haloes accreted at  $z_m = 1$ , and only 10{20 percent of haloes accreted at  $z_m = 2$ , whereas we predict survival rates of 90 percent or 60{80 percent for these redshifts. Some of the discrepancy is simply due to resolution; Gao et al. require more than 10 bound particles to track a halo, which eliminates those systems that retain less than 3{10 percent of their infall mass (for the two mass ranges shown in their plot). Overall, however, the numerical results find a systematically higher disruption rate than we predict. They find that systems accreted at  $z_m = 0.5$  and 1 retain 40 percent and 25 of their infall mass respectively, (Gao et al. 2004b, Fig. 13), whereas we predict the same systems should retain 55 and 45 percent of their infall mass. We will discuss the possible reasons for this disagreement further in paper III.

The lower left-hand panel shows how subhaloes remain roughly stratified within the main system, as a function of their merger epoch (line styles are as in the top left-hand panel). Recently merged systems are close to the ( $z = 0$ ) virial radius, or may even be past it as they go through the first apocentre of their orbit. Older systems are found at progressively smaller radii, reflecting the size of the main system when they first fell into it. In particular, systems which merged before  $z = 2$  and have survived to the present day are typically located at  $0.1\{0.2 r_{\text{vir},m}$ . For the average halo,  $r_{\text{vir}}(z) = r_{\text{vir}}(z = 0) = 0.4$  at  $z = 1$ , 0.22 at  $z = 2$ , 0.085 at  $z = 4$ , and 0.045 at  $z = 6$ , so in fact surviving systems stay close to the virial radius of the halo at the time they fell in. Finally, the lower right-hand panel shows the same stratification in terms of the time elapsed since  $z_m$ , emphasising the synchronised pericentric passage of subhaloes accreted within the past few Gyr, and the apocentric passage of systems accreted 4{5 Gyr ago.

In summary, recently accreted subhaloes (e.g. those with  $z_m < 1$ ) are typically found at  $0.5\{1 r_{\text{vir}}$ . Roughly 90 percent have survived mass loss and tidal heating, and on average they retain 50{100 percent of the mass they had at infall. The oldest systems (e.g. those with  $z_m > 2$ , which fell in 11 Gyr ago) are typically found at  $0.1\{0.2 r_{\text{vir}}$ . Depending on which model we consider, 40{90 percent of them survive, but they typically retain only 20{30 percent of the mass they had at infall.

<sup>3</sup>  $P_{\text{rad}} = 2\pi / \Omega$ , where  $\Omega = (v_c = r_{\text{vir}})(1 + d \ln M / d \ln r)^{1/2}$  is the epicyclic frequency at the virial radius; see paper I.

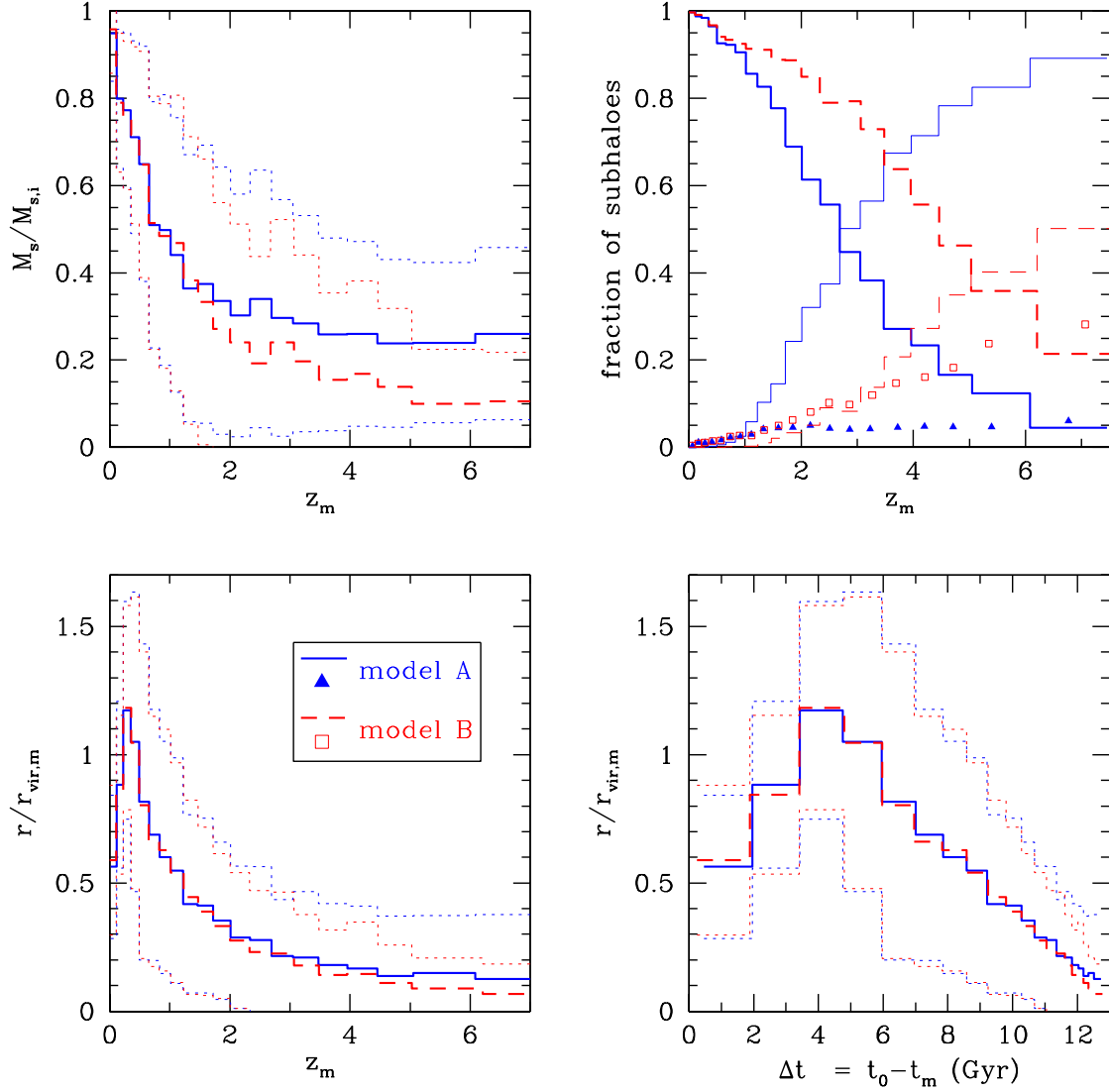


Figure 9. Subhalo properties as a function of merger epoch. Thick solid and dashed lines indicate the mean values for models A and B respectively; the dotted lines indicate the 1- $\sigma$  scatter in each bin. The top-left hand panel shows the fraction of mass remaining. The top right-hand panel shows the fraction of subhaloes that survive (thick lines), that have been disrupted (thin lines), or that have fallen in (points). The lower left-hand panel shows the radial position relative to the virial radius versus merger epoch, and the bottom right-hand panel shows the same quantity as a function of the time elapsed since  $z_m$ .

## 5.2 Other correlations

### 5.2.1 Correlations with mass

The strong dependence of subhalo properties on merger epoch seen in Fig. 9 introduces correlations between other subhalo properties. Fig. 10, for instance, shows how the degree of stripping, the fractions of surviving, disrupted or centrally merged subhaloes, the merger epoch, or the number of orbits spent in the main halo (four panels, clockwise from top left) depend on the mass of the subhalo. Line and point styles are as in Fig. 9. The vertical dot-dashed line indicates the mass resolution of the merger tree. Above this resolution limit, the degree of stripping depends only weakly

on mass (top left panel). More specifically, the most massive subhaloes are systematically younger and therefore less stripped, but otherwise the average degree of stripping is almost independent of mass.

The fraction of surviving or disrupted systems is also roughly independent of mass (top right panel), although dynamical friction causes a greater fraction of the massive subhaloes to fall into the centre of the main system (points). On the other hand, the average merger epoch (lower right) or equivalently the average number of orbits spent in the main halo (lower left) are strongly correlated with subhalo mass, tracking the increasing mass scale of the mergers that form the main halo. Subhaloes below the resolution limit of the

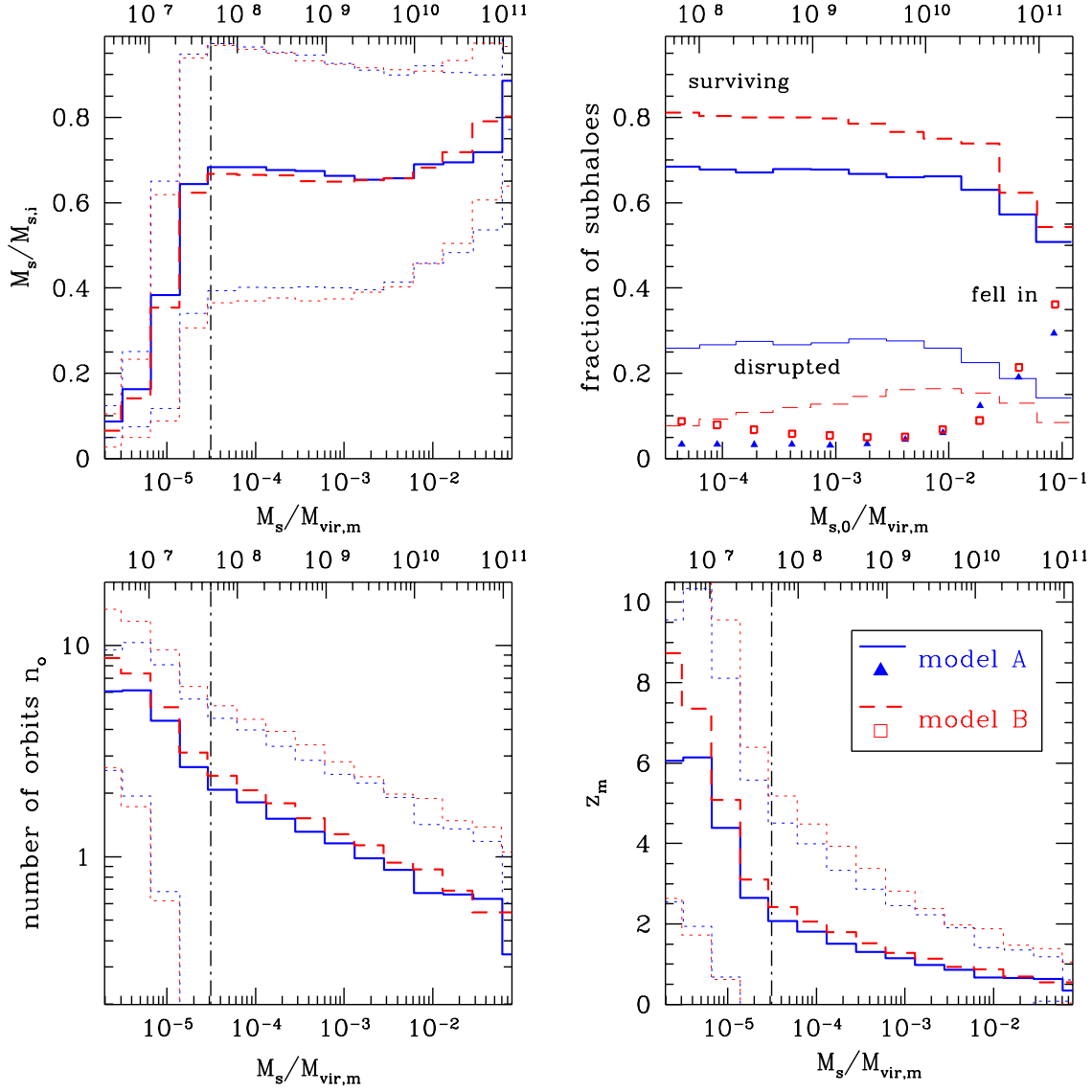


Figure 10. Subhalo properties as a function of mass. Thick solid and dashed lines indicate the mean values for models A and B respectively; the dotted lines indicate the 1- $\sigma$  scatter in each bin. The top-left hand panel shows the fraction of mass remaining. The top right-hand panel shows the fraction of subhaloes that survive (thick lines), that have been disrupted (thin lines), or that have fallen in (points). The bottom left-hand panel shows the average number of orbits spent in the main halo, while the bottom right-hand panel shows the average merger epoch. The dot-dashed line indicates the mass resolution limit of the original merger trees.

merger trees (to the left of the dot-dashed lines) have mainly been stripped, as indicated in the top left panel<sup>4</sup>. They are older than the average subhaloes in that mass range would be if the merger tree extended to a lower mass limit, as indicated by the break in the mean mass-redshift relation in the bottom right panel.

Overall, massive systems have typically merged since a redshift of 1. Roughly 10 percent have been disrupted by repeated mass loss, while 30{40 percent have been disrupted

by falling into the centre of the main system, such that only 50 percent survive. Those that do survive have only spent 1{2 orbits in the main system, and retain 70{90 percent of their infall mass. Low-mass systems are older ( $z_m > 2$ ) and have spent up to 4{5 orbits in the main system. 70{80 percent of them survive, and those that do retain 65 percent of their mass on average (with a 1- $\sigma$  scatter of 0.35{0.95 for individual systems). As before, numerical simulations generally find slightly higher rates of mass loss and disruption. De Lucia et al. (2004, Fig. 11), for instance, find that their subhaloes retain only 40{50 percent of their infall mass on average. Nagai & Kravtsov (2004) also find a somewhat lower value for the retained mass fraction as a function of radius

<sup>4</sup> To avoid boundary effects at the mass resolution limit, the merger trees do include some haloes below  $5 \times 10^7 M_\odot$ , but are very incomplete below this limit.

(cf. their Fig. 4 versus the top left-hand panel of Fig. 10), but their values are expressed in terms of the maximum mass a subhalo had at any point in its merger history (essentially our ‘original mass’), and are thus hard to compare directly. Given a mean mass loss rate of  $\sim 20\{30$  percent for systems before they enter the main system, our results appear to be similar to theirs. On the other hand, Gillet al. (2004b) find similar results for the number of orbits fairly massive satellites have spent in the main system (see their Fig. 6). We will compare our results with simulations in more detail in paper III.

### 5.2.2 Correlations with position

Finally, the increasing size of satellite orbits as a function of time will produce correlations between radial position in the halo and other subhalo properties. Fig. 11 shows the average degree of stripping, the average merger time, the average merger epoch, and the number of orbits subhaloes have spent in the main system as a function of radial position (four panels, clockwise from upper left). Line styles are as in Figs. 9 and 10. These distributions have interesting implications for the dynamical evolution of the central regions of haloes. They indicate, for instance, that subhaloes in the central  $2\{3$  percent of the virial radius (roughly  $6\{10$  kpc, for the Milky Way) have been there for  $10\{12$  Gyr (or since a redshift of  $2\{6$ ), completing tens of orbits and losing 90 percent of their infall mass through tidal stripping. We also note that the difference between models A and B increases for central subhaloes; in model A the average surviving mass fraction is constant and equal to  $\sim 20$  percent in the central 5 percent of the halo, while in model B it continues to decrease at small radii, reaching 5 percent at  $0.02 r_{\text{vir},m}$ . (The sudden change in the distributions at  $0.02 r_{\text{vir},m}$  occurs because we have considered systems that pass within  $0.01 r_{\text{vir},m}$  of the centre of the main halo to have fallen in and been disrupted, as explained in section 2.)

On the other hand, subhaloes close to  $r_{\text{vir},m}$  have typically merged with the main system at  $z_m < 1$  and have completed only  $2\{3$  orbits or less. They have generally been in the main system less than  $6\{7$  Gyr, and retain  $60\{90$  percent of their mass. At these large radii, the results of models A and B are very similar. Gao et al. (2004b) find similar results for subhaloes close to the virial radius in simulations (cf. their Fig. 15), but at small radii there systems are slightly more stripped and have slightly lower merger epochs.

## 6 GLOBAL AGE INDICATORS

Having determined how the properties of individual subhaloes relate to their age and position within a halo, we will now examine how the cumulative distributions of subhalo properties depend on the merger history of their parent halo. As highlighted recently by Diemand et al. (2004c), cumulative mass functions of logarithmic slope  $-1$  are invariant in simple merger scenarios where all (or at least a fixed fraction, independent of mass) of the subhaloes in the progenitors survive in the final system. If  $10$  systems of mass  $M_0$  each with one subhalo of mass  $10^{-2} M_0$  merge together, for

instance, the result is a system of mass  $M_1$  with ten subhaloes of mass  $10^{-3} M_1$ , and the slope of the mass function will be unchanged.

Even if we assume that the mass function does have this form in some initial population of haloes, subsequent mergers between these haloes may change its shape for several reasons. First, dynamical friction will cause subhaloes with more than a few percent of the mass of their parent to fall into the centre of its potential and be disrupted after a few orbits, truncating the mass function at an upper limit which depends on the age of the system. Accretion or mergers with very small haloes will increase the mass of the main system without adding to its massive substructure, shifting or steepening the mass function. Finally, if a halo is isolated and grows relatively little over some period, tidal mass loss will systematically reduce the mass of its subhaloes, decreasing the amplitude of the mass function.

In summary, the subhalo population evolves through two competing effects: injection and mass loss or disruption. The former occurs only during mergers, while the latter operates at a rate that depends on subhalo mass and on the orbital period of the main system, or equivalently on cosmic time. Thus we expect to see systematic trends in the relative mass function of a halo that correlate with its assembly history. In particular, we expect the amplitude of the relative mass function to be largest when a halo is dynamically ‘young’ (in the sense that it has assembled a large fraction of its mass recently), and smallest when it is dynamically ‘old’, since the subhalo population will gradually be stripped and disrupted during the quiescent periods in a halo’s evolution. In this sense ‘young’ and ‘old’ haloes are analogous to relaxed and unrelaxed galaxy clusters; indeed observations of group and cluster luminosity functions may provide a simple observational test of the evolutionary history and formation rate for haloes of different mass (e.g. Jones et al. 2003; see also Trentham & Tully 2002; Roberts et al. 2004; Donghia & Lake 2004).

Fig. 12 shows how the number of subhaloes in one particular halo is related to its mass accretion history. The top panel shows the mass of the system as a function of time,  $M_m(t)$ , normalised to 1 at the present day. The second panel shows the number of subhaloes in the system over a fixed mass threshold of  $10^{10} M_\odot$  (solid line) or  $10^9 M_\odot$  (dotted line), as well as the total number down to the resolution limit. In each case we have normalised to the number over the same threshold at the present day. Although the patterns are slightly obscured by the small number of massive subhaloes, we see that while the total number of subhaloes tracks the relative mass of the system, the number of massive subhaloes peaks after every major merger. There are two to three times more subhaloes over  $10^{10} M_\odot$  after every major merger in the last 10 Gyr, for instance (solid line). After each merger the number then decreases over  $1\{2$  Gyr, as these subhaloes fall in and are disrupted, or are tidally stripped to the point that they drop below the mass threshold. Comparing the last and second-to-last peaks, there is also a marginal indication that the timescale for this decline increases with time, as we would expect given its scaling with orbital timescales, which in turn scale roughly as the age of the universe (see section 5.1). The dotted line shows similar patterns for slightly less massive subhaloes, although

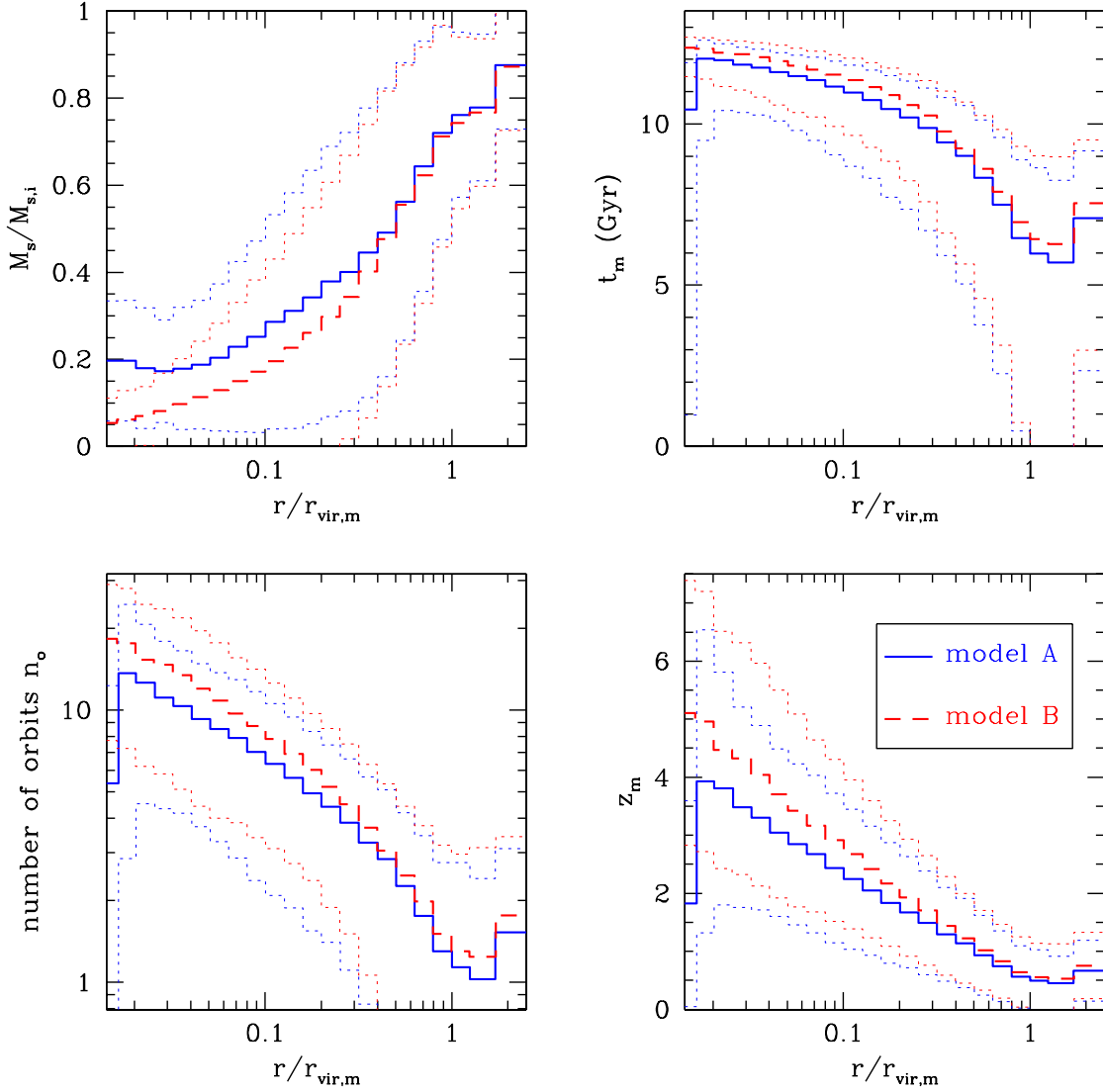


Figure 11. Subhalo Properties as a function of position. Line styles are as in Figs. 9 and 10. The four panels show the average and scatter in the degree of stripping (top left), the merger time (top right), the number of orbits spent in the main system (bottom left) and the merger epoch (bottom right), in different radial bins.

perhaps with a reduced amplitude at early times, and a more gradual decay.

Of course the mass of the main system is changing throughout these events, complicating the interpretation of their effect on the relative mass function. The third panel from the top shows the same quantities as in the second panel, divided by the mass of the main system at that time, and normalised to one at the present day. (In other words, the quantity plotted is the number of subhaloes per unit mass of the main halo at that time that exceed a fixed mass threshold, in units where the present-day value is 1.) The trends described above are now clearer, and we see that even for the lowest mass threshold (dashed line), the number of subhaloes per unit mass (or equivalently the amplitude of

the relative mass function) is 2–3 times larger just after the halo has assembled.

The change in the relative mass function at a given relative, rather than fixed, mass is shown in the bottom panel. For the most massive systems ( $0.5 \times 10^{-2} M_{\text{vir},m}$ , corresponding to the 5 most massive systems at the present day), the amplitude of the relative mass function is an order of magnitude larger at early times, and even for a lower mass threshold ( $0.5 \times 10^{-3} M_{\text{vir},m}$ , corresponding to the 50 most massive systems at the present day), the amplitude is 4–5 times the present-day value at early times. Overall, we conclude that systems which have experienced recent major mergers should have more massive substructure, but that many of these new subhaloes will be destroyed after a few dynamical times, particularly if they are very massive, consistent with

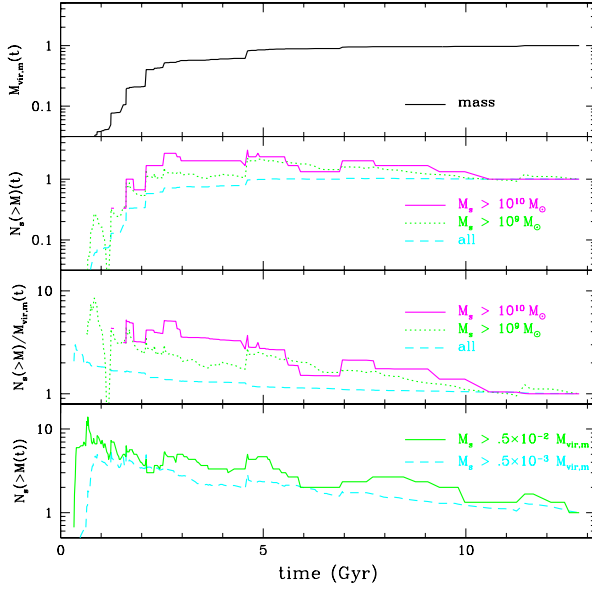


Figure 12. (Top panel) The total mass of a particular halo, relative to the mass at  $z = 0$ . (Second panel) The number of subhalos in the same system over some fixed mass limit, relative to the number at the present day. The dashed, dotted and solid lines are for all subhalos, those more massive than  $10^9 M_\odot$ , and those more massive than  $10^{10} M_\odot$  respectively. (Third panel) the number of subhalos per unit mass of the main halo, relative to the same quantity at the present day. The mass bins are as in the second panel. (Bottom panel) The number of subhalos with more than some fixed fraction of the mass of the main halo at that time, relative to the same quantities at the present day.

the results of paper I. The dependence of substructure on the evolutionary history of the parent halo has been studied recently in numerical simulations by Gill et al. (2004b), who find a similar decay in the number of massive satellites after systems have assembled (e.g. their Fig. 3).

These patterns also suggest that we look for correlations between the amount of substructure in a halo at  $z = 0$  and its formation epoch. Fig. 13 shows the number of subhalos more massive than  $0.5 \cdot 10^{-2}$  or  $0.5 \cdot 10^{-3}$  times the mass of the main system  $M_m$ , as a function of the formation epochs defined in paper I, that is the epochs by which the main progenitor of the system had built up 90, 75, 50 or 10 percent of its total mass<sup>5</sup>. The number of massive systems is strongly correlated with the recent merger history, as indicated by  $z_{90}$ ,  $z_{75}$  or  $z_{50}$ . As expected from the preceding discussion, younger systems have more massive subhalos, the mean number varying by a roughly factor of five over the range of redshifts sampled. The total number of halos down to  $0.5 \cdot 10^{-4} M_{\text{vir},m}$  is also correlated with the recent merger history of the system, or with its overall age, as indicated by

<sup>5</sup> Note that while the expected distribution of formation epochs  $z_f$  cannot be calculated analytically for  $f < 0.5$ , as a tree may have more than one progenitor of this mass, it remains well defined if we always choose to follow the most massive branch at each branching of the tree, and define  $z_f$  as the time when this branch reaches a fraction  $f$  of the total halo mass at  $z = 0$ .

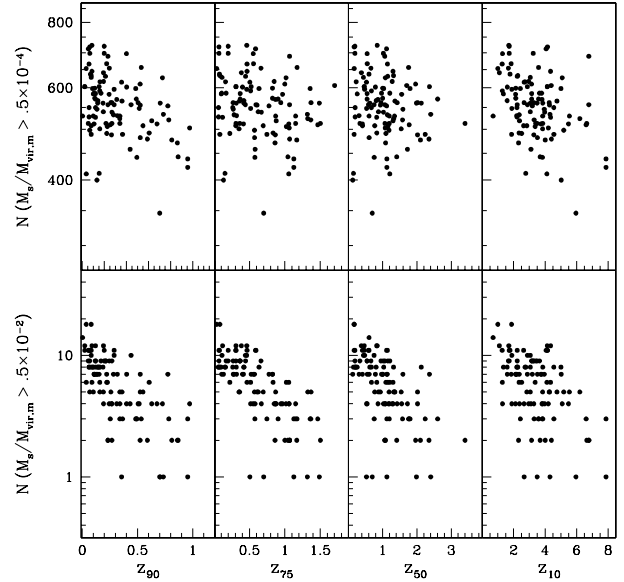


Figure 13. The number of subhalos with more than some fraction of the mass of the main system (at the present day), as a function of the formation epoch of the halo.

$z_{10}$  for instance, although the correlation is weaker and the overall variation in number is less than a factor of two.

Similar correlations for  $z_{50}$  and  $z_{25}$  were reported recently by Gao et al. (2004b, Fig. 8), who also pointed out that the scatter in the correlation may be somewhat larger for  $z_{75}$  or  $z_{90}$ , as these redshifts can be low even for halos formed by recent major mergers of relatively old systems with little internal substructure. We do find somewhat more scatter in the results for  $z_{90}$  than for  $z_{75}$  or  $z_{50}$ , although the trend is not very strong.

These correlations produce systematic changes in the cumulative mass and velocity distributions as a function of formation epoch. Fig. 14 shows the cumulative mass functions for systems binned by formation epoch  $z_{75}$ . The four bins:  $z_{75} < 0.3$ ,  $z_{75} = 0.3\{0.55$ ,  $z_{75} = 0.55\{1.00$ , and  $z_{75} > 1.00$ , were chosen to produce roughly equal numbers of halos in each bin. The effect seen in Fig. 12 is visible here as well; old systems have a steeper mass function that is more strongly truncated at the high mass end, relative to the younger systems. (We note that the overall scatter in the mass of the most massive satellite shown in Fig. 14 is very similar to that found by De Lucia et al. 2004 for halos of a similar mass { cf. their Fig. 4.) In themass range  $M_s = M_{\text{vir},m} = 10^{-3}\{10^{-4}$ , the mean slope of the cumulative mass function is  $-0.89, -0.92, -0.98$  and  $-1.09$  for the four bins respectively. As expected from Fig. 13, there is only a slight change in the amplitude of the mass function at the low mass end, although this might be stronger if we had binned the halos by  $z_{50}$  or  $z_{10}$ . Overall, the systematic dependence of the mass function on dynamical age may explain some of the variation in cumulative mass and velocity functions reported in recent simulations (e.g. De Lucia et al. 2004; Gao et al. 2004b).

The systematic change in the mass function is particularly important when calculating the fraction of the halo



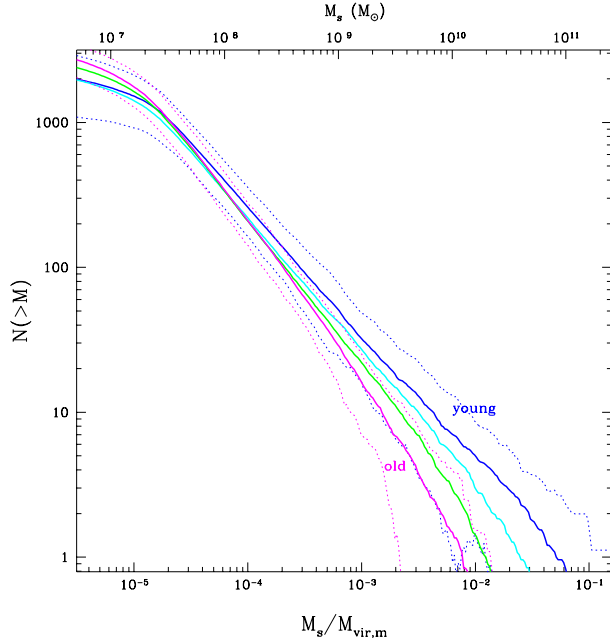


Figure 14. Cumulative mass functions for systems binned by formation epoch  $z_{75}$ . The four solid lines are for  $z_{75} < 0.3$ ,  $z_{75} = 0.3-0.55$ ,  $z_{75} = 0.55-1.00$ , and  $z_{75} > 1.00$  from right to left at the high mass end. The thin dotted lines show the 2- $\sigma$  halo-to-halo scatter for haloes in the first and last bins.

mass contained in substructure, since it is dominated by massive subhaloes. Fig. 15 shows how this quantity varies by a factor of 4 over the age bins considered above. As we discuss in paper III, the systematic dependence of the amount of substructure on the dynamical history of the halo may account for part of the discrepancy between numerical substructure mass functions and the semi-analytic predictions. Only very recently have high-resolution results been available for sufficiently many systems to test for halo-to-halo variations. Fig. 7 of Gao et al. (2004b) or Fig. 1 of Gill et al. (2004b) show how much the mass fraction in substructure varies from halo to halo, for instance, in high-resolution CDM simulations. The scatter is similar to that shown in Fig. 15, although Gao et al. (2004b) finds a substantially lower mean fraction, whereas Gill et al. (2004b), using an adaptive group finder, finds results closer to those shown here. Finally we note that the scatter in the mass fraction from halo-to-halo can be very large, as a few of our systems have subcomponents with a substantial fraction (20-30 percent) of the total halo mass (this also explains why the average cumulative mass fraction in Fig. 15 is already substantial at large masses).

## 7 GROUPING AND ENCOUNTERS

### 7.1 Modelling group dynamics

As discussed in paper I, our semi-analytic model contains higher-order information about substructure merging into the main system. As a result of the pruning process, we can identify in the final merger tree groups of subhaloes which should be kinematically associated with one another when they first fall in, because they represent substructure from a

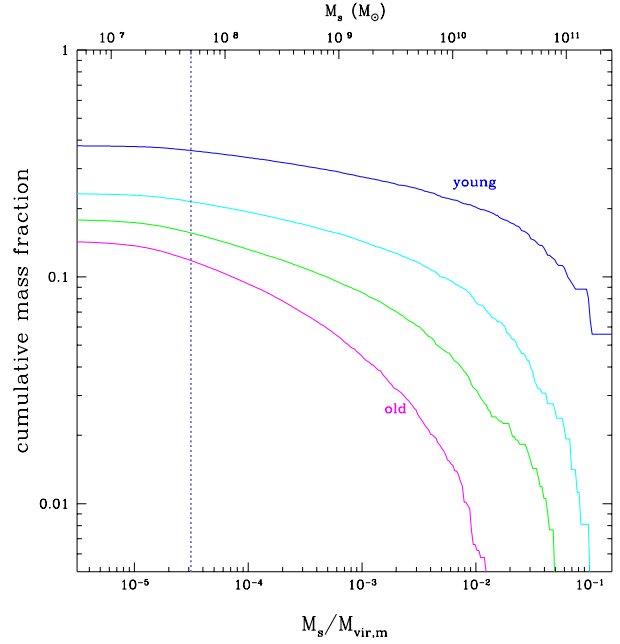


Figure 15. The fraction of the mass within the virial radius contained in subhaloes of mass  $M$  or larger. The subhaloes have been binned by formation epoch  $z_{75}$ , as in Fig. 14, with age increasing from top to bottom.

single merging system. These kinematic groups are assigned a mean orbit, and each member of the group is given an initial offset in position and in velocity relative to this mean, as described in paper I. In this way we reproduce approximately the patterns found in spatially resolved simulations of halo mergers.

An average system contains many kinematic groups, although most have only a few members. Fig. 16 shows a histogram of the average number of groups versus the number of members in the group. It is roughly a power law of slope  $-1.75$ , with on the order of a hundred groups in the average halo, including one or two large groups with 10 members or more.

As groups fall in and evolve in the main system, their members will be scattered and disrupted, particularly since we do not include the self-gravity of a group in our orbital calculations (except in the approximate sense that the haloes which are most tightly bound to their parent system are subsumed in the parent during the pruning of the merger tree). We can study the evolution of groups with time by plotting the spatial dispersion and velocity dispersion of groups as a function of their age. Fig. 17 shows these dispersions, normalised to the virial radius  $r_{\text{vir},m}$  and the virial velocity  $v_{\text{vir},m}$  of the main system, at  $z = 0$ . For each group, the size of the symbol indicates the number of members (which is roughly correlated with the total group mass), while the four panels show groups with successively earlier infall times, corresponding to systems which are falling in for the first time (top left), systems which have passed through pericentre once (top right), systems which have completed 2-10 orbits (lower left) and systems which have completed more than 10 orbits (lower right).

In our model for grouping, groups start out with  $v = v_c$ ,  $r = r_{\text{vir},m}$ , each dispersion being proportional to

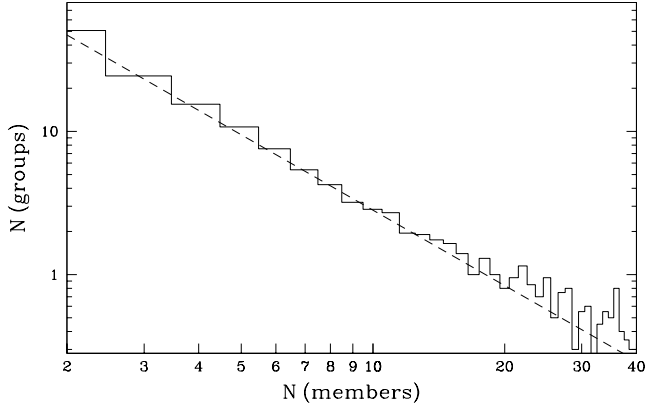


Figure 16. The average number of kinematic groups per halo with a given number of members. The dashed line has a slope of  $-1.75$ .

the cube root of the mass of the group (see paper I, section 5.3). This corresponds to the dashed line running diagonally across each panel. The four panels illustrate several phases in the subsequent evolution of group dynamics. By the time of their first pericentric passage, recently merged groups have been compressed and heated slightly such that  $r = r_{\text{vir},m} < r_v = v_c$ , and thus they lie to the left of the dashed line (top left panel). As they continue to orbit, conservation of phase-space density turns the scatter in positions into a scatter in velocities, so the groups move back towards the dashed line. Slightly older groups (top right panel) continue to experience this orbital heating, moving them upwards in the plot. As groups evolve through many orbits, (lower left panel) their velocity dispersion increases until it reaches the velocity dispersion of the main system; at this point, any information about orbital correlations within the group has effectively been lost. The members of old groups have systematically smaller orbits, however, as discussed in paper I. Thus the spatial dispersion of the oldest groups (lower right panel) is smaller relative to virial radius of the main system at the present day.

## 7.2 Encounters and harassment

While we cannot treat interactions between subhaloes realistically in our model, we can get an indication of their relative importance by tagging close encounters between subhaloes, that might lead to orbital scattering, mass loss or disruption. The number of encounters recorded will depend strongly on the maximum impact parameter  $b_{\text{max}}$  used to define a close encounter. We choose the impact parameter such that the close encounters we record have roughly the same tidal effect as a pericentric passage in the subhalo's orbit. This corresponds to choosing  $b_{\text{max}}$  such that the mean density of the larger member of the interacting pair interior to  $b_{\text{max}}$  is comparable to the density of the main system interior to the pericentre of a typical subhalo orbit. Assuming self-similarity between the inner regions of the subhaloes and the inner part of the main system, this will be the case for encounters at impact parameters less than a few times the peak circular velocity radius of the larger subhalo,  $r_p$ . Thus it is useful to define encounter statistics in terms of

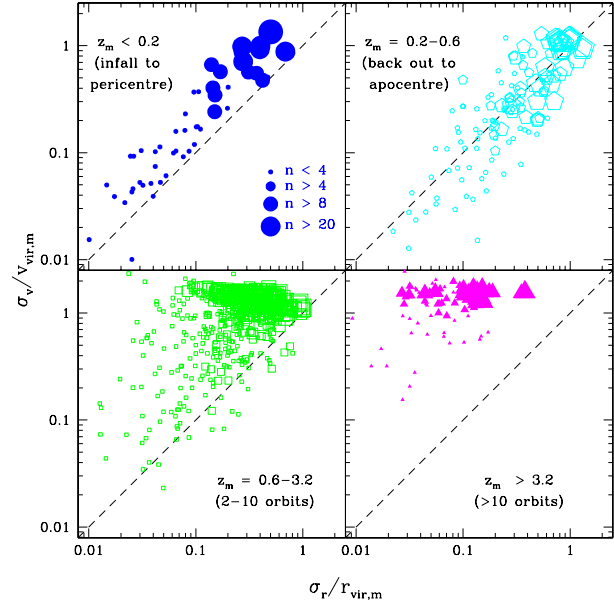


Figure 17. The spatial dispersion and velocity dispersion of kinematic groups in a set of haloes (at  $z = 0$ ). The size of the symbol shows the number of members, as indicated in the first panel. Through phase mixing and subsequent virialisation, successively older groups have moved to the right (top two panels) and then to the top of the plot (bottom two panels).

the scaled impact parameter  $x = b/r_p$ , where  $r_p$  is the peak radius of the more massive halo in an interacting pair.

The top panel of Fig. 18 shows how the number of encounters varies with  $x$ . We have normalised the number of encounters by the total number for  $x < 5$ . The cumulative number is roughly a power-law:  $N(< x) = N_0 x^{2.5}$ . We expect encounters with more massive systems at  $x < 2$  (that is encounters where the haloes overlap at or within each other's peak radii) to heat and strip subhaloes roughly the same way pericentric passages do. In what follows we will refer to such events as 'major' encounters. Overall, find that more than 65 percent of subhaloes have had at least one major encounter defined in this way, and 45 percent have had more than one. The bottom panel of Fig. 18 shows a histogram of the fraction of systems that have had a given number of major encounters.

We note that subhalo encounter rates have also been measured in simulations by Tormen et al. (1998), and more recently by Knebe et al. (2004). While both of these studies find that encounters are common (affecting 60/75 or 30 percent of all systems in the two studies, respectively), it is hard to compare their measured rates directly with ours as each study uses quite different criteria to define an encounter.

Fig. 19 shows the distribution of times at which major encounters occurred (top panel), and the delay between infall and the last major encounter as a fraction of the total length of time the subhalo has been in the main system (bottom panel). Most major encounters occur at fairly early times, and they also usually occur shortly after the subhalo in question first merged into the main system. This is probably because the density of subhaloes within a halo is highest

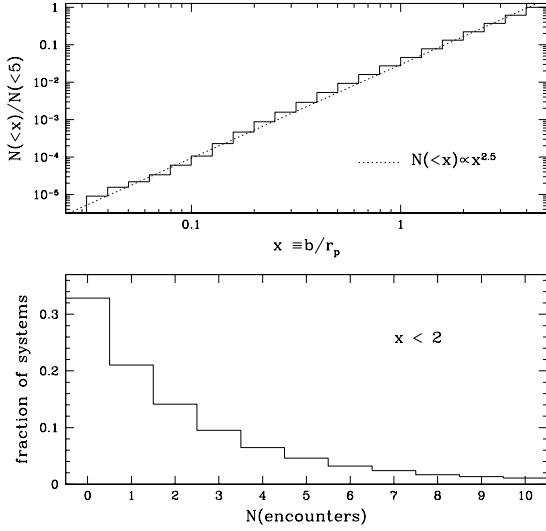


Figure 18. (Top panel) the number of close encounters between haloes with impact parameters less than  $x$  times the peak radius of the larger system,  $r_p$ . The cumulative number goes roughly as  $x^{2.5}$ , as indicated by the dotted line. (Bottom panel) the fraction of systems that have had a given number of encounters with systems of equal or greater mass, at impact parameters of less than twice the peak radius of the more massive system.

at early times or after a recent period of accelerated growth, as discussed in section 6. In particular, collisions and interactions between members of a kinematic group are most likely to occur at the first pericentric passage of the group, when the orbits of its members are focused together. Triggering through collisions, encounters and pericentric passages may play an important role in determining the star-formation histories of the dwarf galaxies of the Local Group, as discussed in Taylor (2002). We will consider this point in more detail in future work.

Since a large fraction of our subhaloes will have had a close encounter with another system of comparable mass by  $z = 0$ , we may be underestimating the extent to which they are tidally heated or stripped. In clusters, the dynamical effect of multiple encounters has been referred to as ‘harassment’ (Moore et al. 1996). We can quantify the possible effect of harassment on the subhalo mass function by stripping from a subhalo the average fraction of its mass it would lose in a pericentric passage, every time it experiences an encounter with a more massive system at an impact parameter of  $b_{\text{max}} = 2r_p$  or less. The motivation for this approximation, as mentioned above, is that the tidal force generated by the two events should be comparable. In the bottom right-hand panel of Fig. 5, we showed the effect of this additional term on the differential mass function. The curve labelled ‘collisions’ corresponds to a case where every subhalo experiencing a collision with a larger subhalo at  $x < 1$  is reduced to a fraction  $f_{\text{st}} = 0.73$  of its mass, as if it had experienced another episode of stripping in the merger tree (see section 2). In the case labelled ‘extreme collisions’, satellites are reduced to  $0.1 f_{\text{st}}$  after every major encounter, leading to immediate disruption of the subhalo in most cases. Overall, the net effect of harassment is fairly small (in the former

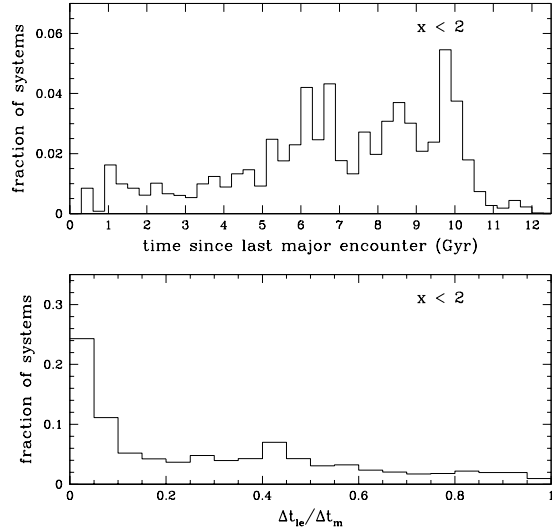


Figure 19. The distribution of times since the last major encounter occurred (top panel), and the time delay between infall and the last encounter  $t_{\text{ie}}$  as a fraction of the total length of time the subhalo has been in the main system,  $t_m$  (bottom panel).

more realistic case it is equivalent to the average subhalo losing an extra 10 to 20 percent of its mass (but since this effect is systematic and probably would occur in a real system, it should be kept in mind when we compare our results with numerical simulations below).

## 8 DISCUSSION

In this paper, we have discussed the basic properties of halo substructure, as predicted by the semi-analytic model of halo formation described in paper I. This model includes several distinct components:

Halo merger histories are generated randomly, using the merger-tree algorithm of Somerville and Kolatt (1999).

The higher order branchings in these trees are ‘pruned’, using the method described in paper I, to determine whether each branch merging with the main trunk contributes a single subhalo or a group of associated subhaloes to the main system. This produces a single list of subhaloes merging with the main system at various redshifts.

Each subhalo from this final list is then placed on a random orbit starting at the virial radius of the main system, and evolved using the analytic model of satellite dynamics described in TB01, experiencing orbital decay due to dynamical friction, and heating and stripping due to tidal forces.

Haloes which were associated with a given parent before pruning fall in together with the parent on similar orbits, as part of a kinematic group.

The properties of the main system change over time, its mass growing according to the merger tree and its concentration changing according to the relations in ENS01.

No baryonic component is included in the models presented here, although one can easily be added, given a prescription for gas cooling and star formation.

Overall accuracy and parametric dependence are important considerations for any semi-analytic model. From paper I, we expect our dynamical model of satellite evolution to predict the properties of individual subhaloes to an accuracy of roughly 20 percent until they have lost a large fraction ( $> 80$  (90 percent) of their original mass. This component of the full semi-analytic model has three principal free parameters: the (halo) Coulomb logarithm,  $\ln \Lambda$ , which determines the strength of dynamical friction, the heating coefficient  $\beta$ , which determines the mass loss rate, and the disruption criterion  $f_{\text{crit}}$ , which determines how long stripped systems continue to survive as bound objects. The values of these parameters were fixed by comparison with the simulations of Velazquez and White (1999) and H03, as described in TB01 and in paper I.

Examining the dependence of our results on the values of these parameters, (in section 4), we conclude that  $\ln \Lambda$  is probably well-enough determined for most applications. The heating parameter  $\beta$  may introduce larger uncertainties, as it was determined from a limited number of simulations with  $10^3$ – $10^4$  particles each. As a result it may be that we overestimate the importance of heating somewhat, and subhalo masses are 20–30 percent larger than we predict. The disruption criterion is also slightly uncertain, although it only affects the survival of highly stripped subhaloes. Here again, we are likely to overestimate the disruption rate, as we are basing our results on simulations of finite resolution.

The rest of the semi-analytic model has no other free parameters, although there are a number of other minor uncertainties, assumptions and approximations in the model. The main assumptions concern the form of the density profile for the main halo, the dependence of halo concentration on mass and redshift, and the distribution of orbital parameters when haloes first merge. The average halo density profile is probably well-enough determined from simulations for most of the applications considered here, as is the initial distribution of satellite orbits. The halo concentrations used here (from ENS01) may be somewhat too small for low-mass haloes (cf. Bullock et al. 2001); in this case we are probably underestimating subhalo masses by 10–15 percent.

The model also makes a number of simplifications or approximations, treating the main halo as spherically symmetric, for instance, and ignoring some of the higher-order terms in subhalo evolution, such as collisions between systems or ‘harassment’. The anisotropy of subhalo orbits has been studied by several authors in recent simulations (e.g. Knebe et al. 2004; Gill et al. 2004b; Aubert, Pichon & Colombi 2004; Benson 2004) and is generally fairly small. We do not expect it to affect our results substantially. Similarly, while the density profiles of simulated CDM haloes are flattened or triaxial to a certain degree, the corresponding potentials are only slightly non-spherical, so we do not expect that flattening will change our results on the spatial distribution of satellites substantially. The higher-order terms in subhalo evolution probably increase mass loss and disruption rates slightly, but the estimates of section 4 suggest this is at most a 10–20 percent effect.

In summary, given the calibration performed in TB01 and paper I, our semi-analytic model has no free parameters, although it includes various assumptions that could be modified, and various simplifications that could be treated in more detail. We expect it to be accurate to roughly 20 per-

cent, the remaining inaccuracy begin due to several competing effects, including possible overestimates of heating and disruption rates, or underestimates of subhalo concentration and mass loss due to encounters. Given this estimated accuracy, it is interesting to compare our results with self-consistent simulations of halo formation.

Overall, the semi-analytic model predicts simple, universal distributions of subhalo mass, circular velocity, and position within the main halo, similar to those seen in simulations. We also predict strong correlations between a subhalo’s merger epoch or formation epoch and its properties, and as a result, between the dynamical history of a halo and the average properties of its substructure. Here again, these are qualitatively similar to trends seen in recent studies of substructure in sets of simulated haloes.

In paper III, we will make a more quantitative comparison between numerical and semi-analytic predictions. We have seen preliminary indications of the results of this comparison in section 5: subhaloes in simulations generally experience more mass loss and are disrupted faster than in the semi-analytic model. While this disagreement could be due to a systematic error in the semi-analytic model, it could also indicate that the simulations are still subject to important resolution effects. We will discuss this issue in more detail in paper III.

## ACKNOWLEDGEMENTS

The authors wish to thank E. Hayashi, S. Ghigna, B. Moore, J. Navarro and T. Quinn for providing data from their simulations for comparison with our model. We also wish to thank E. Hayashi, T. Kolatt, A. Kravtsov, J. Navarro, J. Silk, and S. White for helpful discussions. JET gratefully acknowledges the support of a postgraduate scholarship from the Natural Sciences & Engineering Research Council of Canada (NSERC) during the initial stages of this work, and support from the Leverhulme Trust and from the UK Particle Physics and Astronomy Research Council (PPARC) in the latter stages. AB gratefully acknowledges support from NSERC through the Discovery and the Collaborative Research Opportunities (CRO) grant programs.

## REFERENCES

- Ascasibar, Y., Yepes, G., Muller, V., & Gottlober, S. 2003, *MNRAS*, 346, 731
- Aubert, D., Pichon, C., & Colombi, S. 2004, *MNRAS*, 352, 376
- Benson, A. 2004, *MNRAS*, submitted (astro-ph/0407428)
- Brown, M. L., Taylor, A. N., Bacon, D. J., Gray, M. E., Dye, S., M Eisenheimer, K., & Wolf, C. 2003, *MNRAS*, 341, 100
- Bullock, J. S., Kolatt, T. S., Sigad, Y., Somerville, R. S., Kravtsov, A. V., Klypin, A. A., Primack, J. R., & Dekel, A. 2001, *MNRAS*, 321, 559
- Colin, P., Klypin, A. A., Kravtsov, A. V., & Khokhlov, A. M. 1999, *ApJ*, 523, 32
- Croft, R. A. C., Weinberg, D. H., Bolte, M., Burles, S., Hemquist, L., Katz, N., Kirshen, D., & Tytler, D. 2002, *ApJ*, 581, 20
- De Lucia, G., Kauffmann, G., Springel, V., White, S. D. M., Lanzoni, B., Stoehr, F., Tornen, G., & Yoshida, N. 2004, *MNRAS*, 348, 333
- Demianski, M. & Doroshkevich, A. 2003, *ApJ*, 597, 81

- Desai, V., Dalcanton, J. J., Mayer, L., Reed, D., Quinn, T., & Govomato, F. 2004, *MNRAS*, 351, 265
- Diemand, J., Moore, B., Stadel, J., & Kazantzidis, S. 2004, *MNRAS*, 348, 977
- Diemand, J., Moore, B., & Stadel, J. 2004, *MNRAS*, 290
- Diemand, J., Moore, B., & Stadel, J. 2004, *MNRAS*, 352, 535
- D'Onglia, E., Lake, G. 2004, *ApJ*, in press (astro-ph/0309735)
- Eke, V. R., Navarro, J. F., & Steinmetz, M. 2001, *ApJ*, 554, 114 (ENS01)
- Evrard, A. E. et al. 2002, *ApJ*, 573, 7
- Fukushige, T., Makino, J., 2001, *ApJ*, 557, 533
- Fukushige, T. & Makino, J. 2003, *ApJ*, 588, 674
- Fukushige, T., Kawai, A., & Makino, J. 2004, *ApJ*, 606, 625
- Gao, L., De Lucia, G., White, S. D. M., & Jenkins, A. 2004, *MNRAS*, 352, L1
- Gao, L., White, S. D. M., Jenkins, A., Stoehr, F., & Springel, V. 2004, *MNRAS*, submitted (astro-ph/0404589)
- Ghigna, S., Moore, B., Govomato, F., Lake, G., Quinn, T., & Stadel, J. 1998, *MNRAS*, 300, 146 (G98)
- Ghigna, S., Moore, B., Govomato, F., Lake, G., Quinn, T., & Stadel, J. 2000, *ApJ*, 544, 616 (G00)
- Gill, S. P. D., Knebe, A., & Gibson, B. K. 2004a, *MNRAS*, 351, 399
- Gill, S. P. D., Knebe, A., Gibson, B. K., & Dopita, M. A. 2004b, *MNRAS*, 351, 410
- Gottlober, S., Klypin, A., & Kuvshinov, A. V. 2001, *ApJ*, 546, 223
- Gottlober, S., Lokas, E. L., Klypin, A., & Homann, Y. 2003, *MNRAS*, 344, 715
- Govomato, F., Ghigna, S., Moore, B., 2001, in *ASP Conf. Ser.* 245: *Astrophysical Ages and Times Scales*, 469
- Hamana, T. et al. 2003, *ApJ*, 597, 98
- Hatton, S., Devriendt, J. E. G., Ninin, S., Bouchet, F. R., Guiderdoni, B., & Vibert, D. 2003, *MNRAS*, 343, 75
- Hayashi, E., Navarro, J. F., Taylor, J. E., Stadel, J., & Quinn, T. 2003, *ApJ*, 584, 541 (H03)
- Hoeft, M., Muckel, J. P., & Gottlober, S. 2004, *ApJ*, 602, 162
- Hoekstra, H., Yee, H. K. C., Gladders, M. D., Barrientos, L. F., Hall, P. B., & Infante, L. 2002, *ApJ*, 572, 55
- Jarvis, M., Bernstein, G. M., Fischer, P., Smith, D., Jain, B., Tyson, J. A., & Wittman, D. 2003, *AJ*, 125, 1014
- Jing, Y. P., Suto, Y. 2002, *ApJ*, 574, 538
- Jones, L. R., Ponman, T. J., Horton, A., Babul, A., Ebeling, H., & Burke, D. J. 2003, *MNRAS*, 343, 627
- Kaumann, G., Colberg, J. M., Diaferio, A., & White, S. D. M. 1999, *MNRAS*, 303, 188
- Kazantzidis, S., Mayer, L., Mastropietro, C., Diemand, J., Stadel, J., & Moore, B. 2004, *ApJ*, 608, 663
- Kochfar, S., & Burkert, A. 2003, *MNRAS*, submitted (astro-ph/0309611)
- Kim, T.-S., Viel, M., Haehnelt, M. G., Carswell, R. F., & Cristiani, S. 2004, *MNRAS*, 347, 355
- Klypin, A., Gottlober, S., Kuvshinov, A. V., & Khokhlov, A. M. 1999, *ApJ*, 516, 530
- Klypin, A., Kuvshinov, A. V., Valenzuela, O., & Prada, F. 1999, *ApJ*, 522, 82
- Klypin, A., Kuvshinov, A. V., Bullock, J. S., & Primack, J. R. 2001, *ApJ*, 554, 903
- Klypin, A., Homann, Y., Kuvshinov, A. V., & Gottlober, S. 2003, *ApJ*, 596, 19
- Knebe, A., Gill, S. P. D., Gibson, B. K., Lewis, G. F., Ibata, R. A., & Dopita, M. A. 2004, *ApJ*, 603, 7
- Lin, W. P., Jing, Y. P., & Lin, L. 2003, *MNRAS*, 344, 1327
- Miller, A. H., McIntosh, D. H., Katz, N., Weinberg, M. D., preprint (astro-ph/0304005)
- Mather, H., Lemson, G., Springel, V., Kaumann, G., White, S. D. M., Eldar, A., & Dekel, A. 2002, *MNRAS*, 333, 739
- Moore, B., Katz, N., & Lake, G. 1996, *ApJ*, 457, 455
- Moore, B., Katz, N., Lake, G., Dressler, A., & Oemler, A. 1996, *Nature*, 379, 613
- Moore, B., Govomato, F., Quinn, T., Stadel, J., & Lake, G. 1998, *ApJ*, 499, L5 (M98)
- Moore, B., Ghigna, S., Govomato, F., Lake, G., Quinn, T., Stadel, J., & Tozzi, P., 1999, *ApJ*, 524, L19 (M99a)
- Moore, B., Quinn, T., Govomato, F., Stadel, J., & Lake, G. 1999, *MNRAS*, 310, 1147 (M99b)
- Nagai, D., Kuvshinov, A. V. 2004, *ApJ*, submitted (astro-ph/0408273)
- Navarro, J. F., Frenk, C. S., & White, S. D. M., 1996, *ApJ*, 462, 563
- Navarro, J. F., Frenk, C. S., & White, S. D. M., 1997, *ApJ*, 490, 493
- Navarro, J. F., et al. 2004, *MNRAS*, 349, 1039
- Okamoto, T. & Habe, A. 1999, *ApJ*, 516, 591
- Percival, W. J. et al. 2001, *MNRAS*, 327, 1297
- Percival, W. J., Scott, D., Peacock, J. A., & Dunlop, J. S. 2003, *MNRAS*, 338, L31
- Power, C., Navarro, J. F., Jenkins, A., Frenk, C. S., White, S. D. M., Springel, V., Stadel, J., & Quinn, T. 2003, *MNRAS*, 338, 14
- Press, W. H., & Schechter, P. 1974, *ApJ*, 187, 425
- Reed, D., Gardner, J., Quinn, T., Stadel, J., Fardal, M., Lake, G., & Govomato, F. 2003, *MNRAS*, 346, 565
- Reed, D., Govomato, F., Quinn, T., Gardner, J., Stadel, J., Lake, G. 2004, *MNRAS*, submitted (astro-ph/0406034)
- Rhodes, J., Refregier, A., Collins, N. R., Gardner, J. P., Groth, E. J., & Hill, R. S. 2004, *ApJ*, 605, 29
- Roberts, S., et al. 2004, *MNRAS*, 352, 478
- Spergel, D. N. et al. 2003, *ApJS*, 148, 175
- Springel, V., White, S. D. M., Tornen, G., & Kaumann, G. 2001, *MNRAS*, 328, 726
- Stadel, J. 2001, Ph.D. thesis, University of Washington
- Stoehr, F., White, S. D. M., Tornen, G., & Springel, V. 2002, *MNRAS*, 335, L84
- Tasitsioudis, A., Kuvshinov, A. V., Gottlober, S., & Klypin, A. A. 2004, *ApJ*, 607, 125
- Taylor, J. E. 2002, Ph.D. thesis, University of Victoria (<http://www.library.com/dissertations/fullcit/NQ62530>)
- Taylor, J. E. & Babul, A. 2001, *ApJ*, 559, 716
- Taylor, J. E. & Babul, A. 2004a, *MNRAS*, 348, 811 (paper I)
- Taylor, J. E. & Babul, A. 2004b, *MNRAS*, submitted (paper III)
- Taylor, J. E., & Navarro, J. F. 2001, *ApJ*, 563, 483
- Tegmark, M., et al. 2004, *ApJ*, 606, 702
- Tornen, G. 1997, *MNRAS*, 290, 411
- Tornen, G., Diaferio, A., & Syer, D. 1998, *MNRAS*, 299, 728
- Trentham, N., & Tully, R. B. 2002, *MNRAS*, 335, 712
- van Kampen, E. 1995, *MNRAS*, 273, 295
- Van Aerbeke, L., Mellier, Y., Pello, R., Pen, U.-L., McCracken, H. J., & Jain, B. 2002, *A&P*, 393, 369
- Velazquez, H., & White, S. D. M. 1999, *MNRAS*, 304, 254
- Wambsganss, J., Bode, P., & Ostriker, J. P. 2004, *ApJL*, 606, L93
- Weller, J., Ostriker, J. P., & Bode, P. 2004, *MNRAS*, submitted (astro-ph/0405445)
- Yahagi, H., Nagashima, M., & Yoshii, Y. 2004, *ApJ*, 605, 709
- Yoshida, N., Sheth, R. K., & Diaferio, A. 2001, *MNRAS*, 328, 669
- Zhao, D. H., Mo, H. J., Jing, Y. P., & Bower, G. 2003, *MNRAS*, 339, 12
- Zhao, D. H., Jing, Y. P., Mo, H. J., & Bower, G. 2003, *ApJL*, 597, L9